Equilibrium and kinetic phenomena in a stiff homopolymer and possible applications to DNA

Yu. A. Kuznetsov,[a] E. G. Timoshenko,[b] and K. A. Dawson
Theory Group, Centre for Soft Condensed Matter and Biomaterials, Department of Chemistry, University College Dublin, Dublin 4, Ireland

(Received 17 May 1996; accepted 22 July 1996)

We study the bead-and-spring model of a stiff chain using a self-consistent mean-field approach. For high stiffness parameter the system may undergo a transition to the phase in which the globule acquires a toruslike shape. The phase diagram of the model contains one second- and two first-order transitions meeting at a bicritical point. The stability of the toroidal conformation and scalings of the torus geometry are analyzed. We investigate different kinetic regimes after an instantaneous quench between the extended coil, torus and the spherical globule phases. The kinetic laws that govern these conformational changes are obtained. © *1996 American Institute of Physics.* [S0021-9606(96)52240-3]

I. INTRODUCTION

Recently the problem of the description of kinetics at the collapse transition of a homopolymer in dilute solution has attracted considerable attention. Equilibrium aspects of homopolymers had been thoroughly studied for many years.[1–4] There have been extensive Monte Carlo,[5,6] Langevin,[7] and molecular dynamics[8] simulations for kinetics. On the other hand, in theory, the seminal work by de Gennes,[9] where the collapse process was described phenomenologically, has been partially confirmed and further extended within more systematic treatments using the Gaussian self-consistent nonequilibrium method.[10–13] We regard the main issues in this area of flexible homopolymer chains as essentially resolved and point the reader particularly to Ref. 11.

Briefly then, our previous studies of kinetics were based upon the bead-and-spring model described by the Edwards Hamiltonian.[3] The resulting picture of the necklace mechanism of early stages of kinetics due to the spinodal decomposition in the internal metric of the chain, and some analytical estimates[10,11] for the universal exponents, have been confirmed by Monte Carlo lattice simulations.[6] The characteristic time of the dominant stage of kinetics describing a sort of coarsening has a similar scaling to that envisaged by de Gennes,[9] and later stages involve compaction and more complex processes.[11]

Now, the main observable in this approach is $\mathscr{F}_q(t)\equiv(1/3)\langle|\mathbf{x}_q(t)|^2\rangle$, the ensemble-averaged squared amplitude of the qth Fourier mode ($q=0,\ldots,N-1$, where N is the degree of polymerization) of the monomer positions at time t. This satisfies the nonequilibrium equation of motion,[10]

$$\frac{\zeta_q(t)}{2}\frac{d}{dt}\mathscr{F}_q(t)=k_BT-\Delta V_q(t)\mathscr{F}_q(t), \tag{1}$$

where the time-dependent effective friction, $\zeta_q(t)$, and effective potential, $\Delta V_q(t)$, can be determined self-consistently[14] and expressed through $\mathscr{F}_q(t)$.

These expressions have all been derived on the basis of an effective potential Langevin equation that is discussed at length in our previous papers. However, it is of interest to note that they can be reexpressed in terms of the nonequilibrium extensions of equilibrium thermodynamic quantities. For example, the effective potential may be written as the derivative of the ensemble mean energy [see Eq. (A6) in Ref. 11],

$$\Delta V_q(t)=\frac{2}{3}\frac{\partial\mathscr{E}(t)}{\partial\mathscr{F}_q(t)}. \tag{2}$$

Now, recalling the expression for the entropy $\mathscr{S}$ in the Gibbs–Bogoliubov estimate at equilibrium,

$$\mathscr{S}=\tfrac{3}{2}k_B\sum_q \log\mathscr{F}_q, \tag{3}$$

one may rewrite Eq. (1) via the derivatives of the ''instantaneous'' free energy $\mathscr{A}(t)=\mathscr{E}-T\mathscr{S}$. For this let us first introduce the real positive variable X_q defined as the square root of the positive definite quantity,

$$\mathscr{F}_q(t)=\tfrac{1}{3}\langle|x_q(t)|^2\rangle\equiv\tfrac{1}{3}X_q^2. \tag{4}$$

It is also instructive to use the N-dimensional vector notation, $\mathbf{X}\equiv\{X_q\}$ and introduce the diagonal friction matrix $\zeta_{qq'}=\zeta_q\delta_{qq'}$. Then we shall have,

$$\boldsymbol{\zeta}\cdot\frac{d}{dt}\mathbf{X}(t)=-\frac{\partial\mathscr{A}(t)}{\partial\mathbf{X}(t)}, \tag{5}$$

where the bullet designates the scalar product. Without hydrodynamics $\boldsymbol{\zeta}$ becomes proportional to the unit matrix[15] and this equation acquires a transparent meaning. Note also that the squared radius of gyration is given simply by

$$R_g^2=\tfrac{1}{3}\mathbf{X}\cdot\mathbf{X}. \tag{6}$$

We should emphasize here that only for a simple homopolymer is it possible to present the kinetic equation in

[a]Also at: The Institute of Theoretical and Experimental Biophysics, Russian Academy of Sciences, Pushchino, 142292, Russia.
[b]Electronic address: timosh@fiachra.ucd.ie

the above simple form appealing to extensions of equilibrium notions such as the free energy. For more complex systems, e.g., periodic and random heteropolymers,[16] the generalizations of Eq. (5) may be derived from the Gaussian self-consistent method, but they have a more complicated form and cannot be established from purely phenomenological arguments.

Nevertheless, the form in Eq. (5) is useful for understanding the kinetics of a homopolymer as the evolution in the phase space of the dynamical variables $\mathbf{X}$ against the gradient of the free energy, i.e., in the direction of its deepest descent. Thus, at equilibrium the system is in the absolute minimum. After the quench it happens to be at a nonstationary point and starts moving towards the new absolute minimum of the free energy. If it encounters a metastable minimum on its way it will be trapped there. Some of the metastable minima cease to be such at the new values of the thermodynamic parameters (i.e., after the quench) and typically become saddle points or just valleys with a gentler slope. These will manifest themselves in a characteristic slowing down of the kinetics as it passes through such places. Thus the rate of kinetics could be described by the time derivative of the free energy as well as the modulus of its gradient. Indeed, it is simple to calculate the time derivative of the free energy from Eq. (5)

$$\frac{d}{dt}\mathscr{A}(t) = -\frac{\partial \mathscr{A}}{\partial \mathbf{X}} \cdot \boldsymbol{\zeta}^{-1} \cdot \frac{\partial \mathscr{A}}{\partial \mathbf{X}}. \tag{7}$$

Given the Hamiltonian of the model, V, and provided one can calculate its ensemble average $\mathscr{E}=\langle V\rangle$, the kinetic equations are completely determined and can be numerically studied using the standard technique.[11]

In this paper we shall be interested in how the homopolymer kinetics at the collapse transition is modified due to the effect of stiffness. The stiffness could be introduced into the theory in a number of physically equivalent ways. There is a significant amount of theoretical[17] and experimental[18] literature dealing with various questions about equilibrium properties of rigid chains, the most important practical example of which is DNA. Experimentally, it is well known that DNA can acquire a torus-like shape in its globular state,[4] and that condensation of DNA induced by various agents could lead to even more complicated phases.[18] In theory the torus shape has been predicted in Ref. 19. The physical reason for a torus is clear—a persistent chain has no desire to bend, so it tends to have as large a radius of curvature as possible, consistent with quite close packing of the chain. Nevertheless, to construct a good qualitative theory of such states is not very simple.[17]

In the framework of the bead-and-spring model to account for the stiffness it is sufficient to introduce the bending energy, $\Sigma_n(d^2\mathbf{x}_n/dn^2)^2$, as first proposed by Kratky and Porod in 1949 in Ref. 20 and used by Harris and Hearst in Ref. 21 for the description of DNA. Alternatively, one can use the model of the freely-rotating chain discussed, i.e., in Refs. 22.

Our initial probes of the model revealed a sort of slowing down in kinetics of a stiff chain in agreement with Ref. 13. In addition we should note here that we have earlier observed such kinetic phenomenon in our study of copolymers[16] and only now are the connections becoming clear to us. Further surprises consisted in that it was possible for the same rigidity to produce one, two, or no slow regimes in kinetics by changing the quench depth. By studying the heat capacity, bending energy, and the correlations of monomer positions along the chain, D_m, it has become evident to us that for high rigidity parameter the system may undergo a transition to a new toroidal phase, and also that the kinetics depends crucially on how close one is to the spinodals associated with first order transitions.

This set of conspicuous observations has led us to undertake a more complete study of the effect of stiffness in the kinetics of a homopolymer presented below. We believe that the result is a rather interesting picture relating the equilibrium structure of a persistent chain to its kinetics in an elegant manner.

II. THE MODEL

The Hamiltonian of the model is written as the sum of three contributions: the spring term, the bending energy, and the excluded volume terms,

$$V = V_{\text{springs}} + V_{\text{bend}} + V_{\text{excl.v.}}, \tag{8}$$

$$V_{\text{spring}} = \frac{k_B T}{2l^2} \sum_m (\mathbf{x}_m - \mathbf{x}_{m-1})^2, \tag{9}$$

$$V_{\text{bend}} = \frac{k_B T \lambda}{2l^3} \sum_m (\mathbf{x}_{m+1} + \mathbf{x}_{m-1} - 2\mathbf{x}_m)^2, \tag{10}$$

$$V_{\text{exlc.v.}} = \sum_{L=2}^{\infty} u_L \sum_{m_1 \ldots m_L} \prod_{i=1}^{L-1} \delta(\mathbf{x}_{m_1} - \mathbf{x}_{m_{i+1}}), \tag{11}$$

where l is the bond length, λ/l is the stiffness parameter[3] and u_L are the virial coefficients, with $m_1 \neq m_2 \cdots \neq m_L$.

The ensemble averaged energy is given by,[10]

$$\mathscr{E} = \frac{3k_B T N}{2l^2} \sum_q d_{01}^{(q)} \left(1 + \frac{\lambda}{l} d_{01}^{(q)}\right) \mathscr{F}_q + \sum_{L=2}^{\infty} \hat{u}_L \sum_{m_1 \ldots m_L} (\det \Delta^{(L-1)})^{-3/2}. \tag{12}$$

The second term of this expression is the averaged bending energy $\mathscr{E}_{\text{bend}}$. In this formula $\Delta^{(L-1)}$ is a matrix of the size $L-1$ with the matrix elements,

$$D_{ij}^{(L-1)} = D_{m_1 m_{i+1}, m_1 m_{j+1}} \tag{13}$$

and $\hat{u}_L = u_L/(2\pi)^{3(L-1)/2}$. The correlations $D_{nn',mm'}$ of monomer spatial positions $\mathbf{x}_n$ may be expressed as the Fourier transforms of the normal modes,

$$D_{nn',mm'} = \tfrac{1}{3}\langle (\mathbf{x}_n - \mathbf{x}_{n'})(\mathbf{x}_m - \mathbf{x}_{m'})\rangle = \sum_q d_{nn',mm'}^{(q)} \mathscr{F}_q, \tag{14}$$

$$d_{nn',mm'}^{(q)} = -\tfrac{1}{2}(d_{nm}^{(q)} + d_{n'm'}^{(q)} - d_{nm'}^{(q)} - d_{n'm}^{(q)}), \tag{15}$$

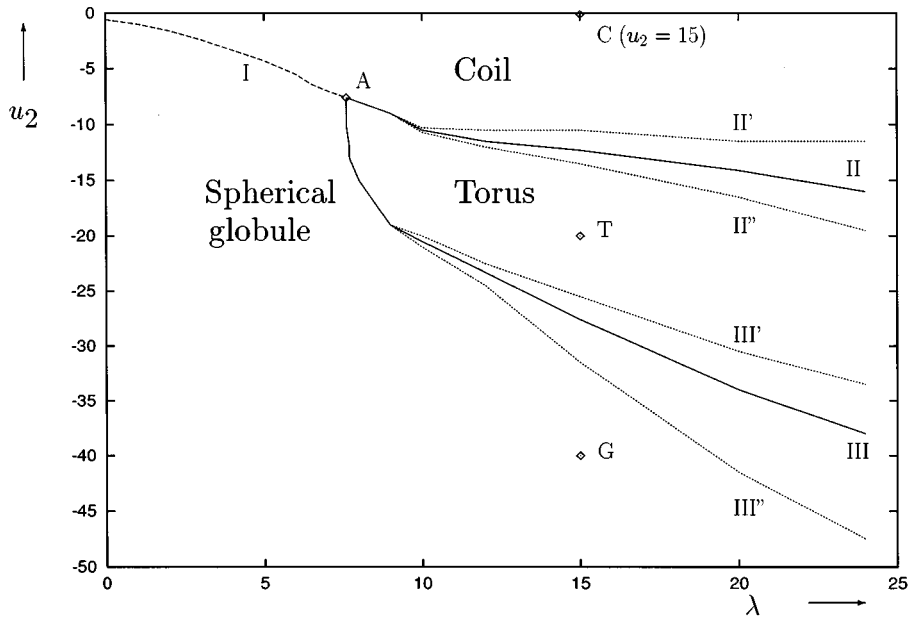

FIG. 1. The phase diagram of a stiff homopolymer in variables of the stiffness parameter λ and the second virial coefficient u_2. Curve I corresponds to the second order phase transition and curves II, III—to the first order transitions. Point A is a bicritical point. Curves II′,II″ and III′,III″ are spinodals. This diagram has been obtained from the data for polymer with the degree of polymerization $N=100$.

with $d_{nm}^{(q)}=|f_n^{(q)}-f_m^{(q)}|^2$ and $f_n^{(q)}=\exp(i2\pi qn/N)$ being the coefficients of the Fourier transform of a ring polymer.[23] Analogously we define the two-point correlations of monomer spatial positions, $D_{nn'}\equiv D_{nn',nn'}$, and for a ring we can write $D_{n-n'}\equiv D_{nn'}$ due to cyclicity.

III. RESULTS

Equations (1), (2), and (12) have been analyzed numerically both for equilibrium and kinetics using the techniques applied a number of times in the past.[11,16] As usual, we restrict ourselves by accounting for the excluded volume effect only up to the three-body interaction, i.e., we assume $u_L=0$ for $L>3$. We shall use the following choice of parameters: $k_BT=1$, $l=1$ and $\zeta_b=1$, which fix the units of measurement of temperature, size and time in the system. In what follows the third virial coefficient is taken $u_3=10$ similar to Ref. 11 unless otherwise stated.

A. Equilibrium considerations

Equilibrium is recovered by setting the time derivatives in Eq. (1) to zero, and this yields the equation for determining possible local minima of the free energy, $\mathscr{A}$. Moreover, one should choose the solution corresponding to the global minimum of $\mathscr{A}$.

1. Numerical analysis

In Fig. 1 we present the phase diagram of the model in variables of the stiffness, λ, and the second virial coefficient, u_2. The coil phase corresponds to extended conformations of the polymer with a large radius of gyration scaling as $R_g \sim N^{\nu_{\rm coil}}$, where the exponent $\nu_{\rm coil}$ is close to the Flory value $\nu_F=3/5$ for a flexible chain,[24] becomes a rigid rod exponent $\nu_{\rm rod}=1$ for a very stiff chain, with a crossover in between.

A new feature here, in comparison to the case of a flexible homopolymer, is that there are two compact states of the system: The spherical globule, which is just a conventional globule, and the toruslike globule. These can be distinguished clearly by the spatial correlations of monomer coordinates along the chain, D_m, exhibited in Fig. 2(a). D_m is a monotonically increasing function of $|m|$ for the spherical globule with the following properties: $D_m \sim |m|^{2\nu_s}$ for small $|m|$, where the ''screened'' exponent is a crossover between the ideal coil and the rigid rod values $1/2\leqslant\nu_s\leqslant 1$; and it saturates to the level scaling as $D_m\sim N^{2/3}$ for sufficiently large $|m|$ (see, e.g., Ref. 4).

However, in what we call the torus phase, this function D_m behaves in a quite unusual manner. For small distances along the chain it is parabolic, $D_m\sim|m|^2$, i.e., represents almost a rigid rod. At the chain index m^* it reaches its maximum value $D_{\rm max}$, then decreases until its minimum $D_{\rm min}$ at (approximately) $m=2m^*$ and further oscillates stabilizing to the level scaling as $N^{2/3}$ (see Table I). In Fig. 2(b) we draw the corresponding dependencies of the amplitudes of the internal modes, $\mathscr{F}_q$, on the chain index q. The oscillations of D_m for the torus are reduced simply to the Lorentzian shape for the Fourier transformed quantities $\mathscr{F}_q$.

These properties can be naturally attributed to the toroidal conformation. Thus a stiff chain, having no point of ''easy bending,'' is nearly straight locally and it wraps around itself forming a hole in the middle of the torus. The chain index m^* is equal to the number of monomers forming a half-period of the first winding starting from the zeroth monomer. Therefore, $D_{\rm max}$ may be interpreted as the mean squared *external* diameter of the torus. By moving from the monomer number m^* to $2m^*$ the first winding is completed. However, because of the excluded volume interaction the

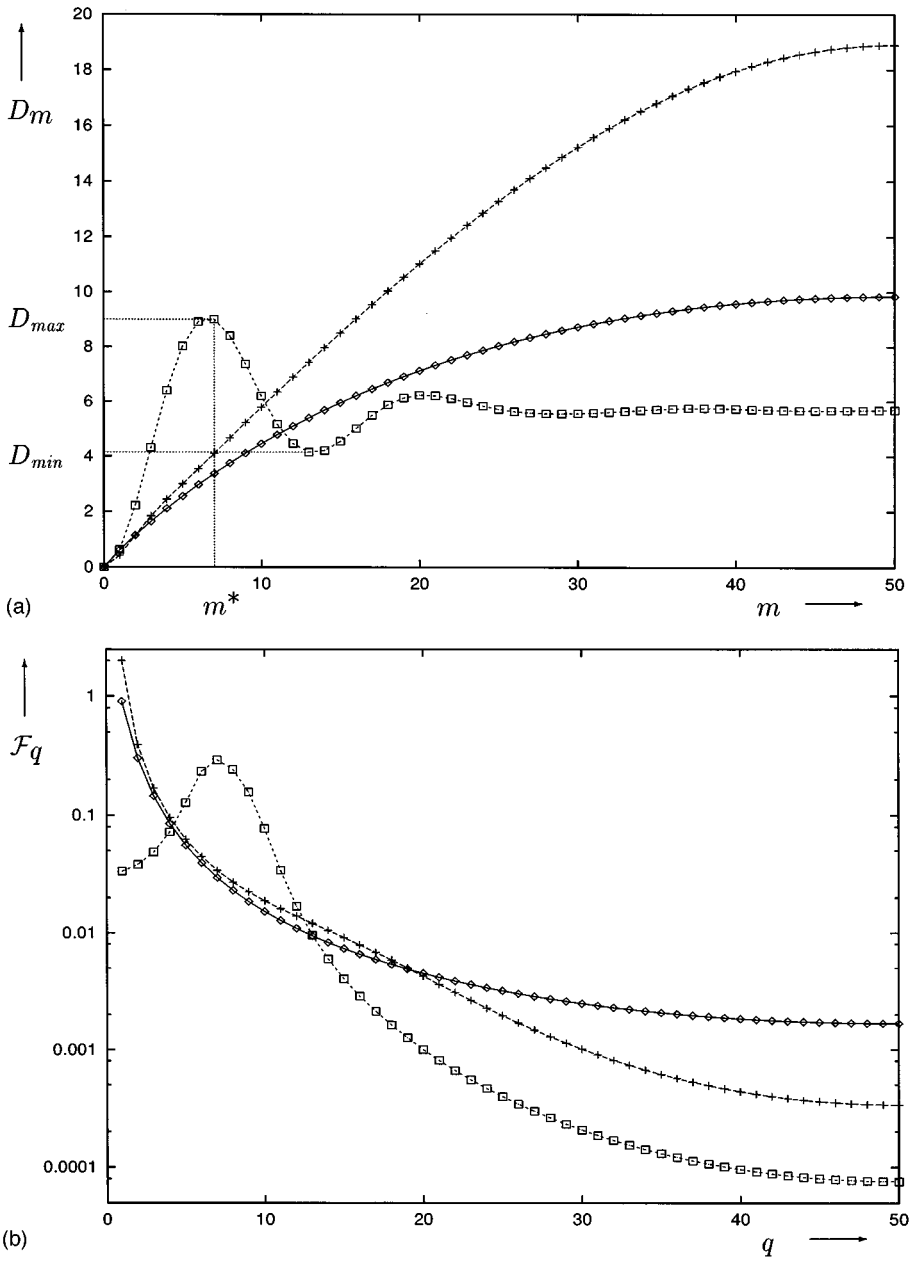

FIG. 2. Plots of the spatial correlations of monomer coordinates D_m vs the chain index m (a) and of the amplitudes of the Fourier modes $\mathcal{F}_q$ (b) vs q for polymer with $N=100$, and $u_2=-25$: pluses—for the stiffness $\lambda=6$ (spherical globule), quadrangles—for $\lambda=24$ (torus), diamonds—for $\lambda=0$ (globule of a flexible homopolymer). Here, m^* denotes the number of units comprising a half of period of the torus, $D_{\min}$ and $D_{\max}$ are the mean squared values of the internal and external diameters of the torus.

chain cannot return to the same coordinate, giving rise in the average to the value $D_{\min}$, which may be related to the mean squared *internal* diameter of the torus.[25] Because of the statistical distribution of a filament within a cross section of the torus, the number of units comprising a complete revolution is not fixed. This leads to a specific ''memory'' effect in the number of windings. Thus the toruslike conformation structure is well represented by the ensemble averaged quantity D_m for the first half-revolution, worse for the whole revolution, and in D_m for $m>2m^*$ the winding information is exponentially quickly obliterated with each next turn. Hence the spatial correlations D_m for large $|m|$ describe mainly the mean squared distances among all possible pairs of monomers, rather than the geometrical properties of an individual torus.

TABLE I. Values of the critical stiffness and parameters of the torus for different degrees of polymerization for $u_2=-20$ and $\lambda=15$. Here, γ denotes the exponent of the appropriate power law in the degree of polymerization.

N	50	70	100	150	200	300	γ
λ_c	10.9	8.0	7.1	6.45	6.0		
$D_{\min}$	5.23	5.43	6.03	6.98	7.85	9.48	0.44±0.02
$D_{\max}$	6.16	7.91	10.01	12.92	15.40	19.80	0.65±0.02

Note that, to characterize the torus conformation, we have preferred to deal with the intrinsic metric quantities, of

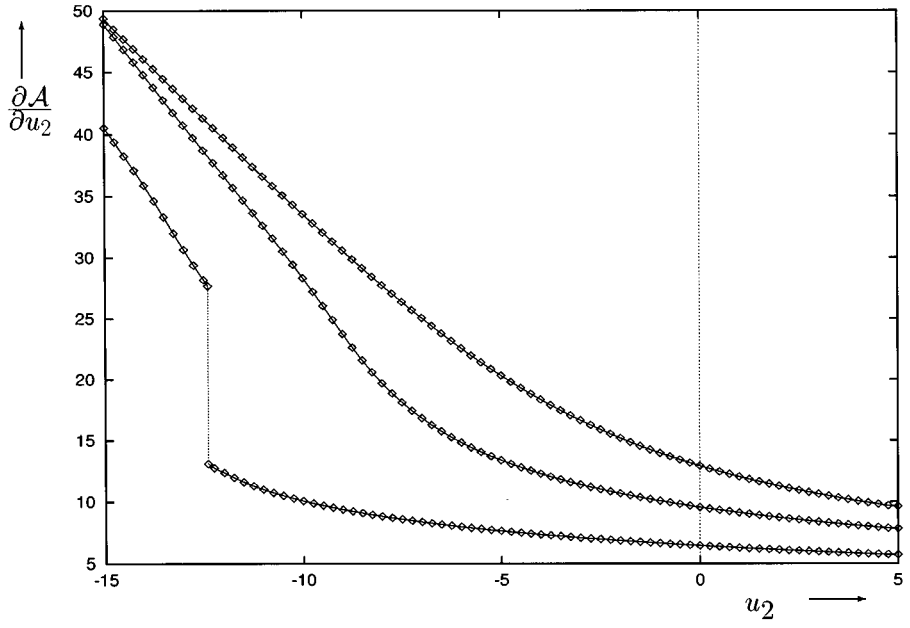

FIG. 3. Plots of the first derivative of the free energy $\mathscr{A}$ with respect to the second virial coefficient u_2 at equilibrium vs the second virial coefficient for different values of the stiffness (from top to bottom): $\lambda=0$ (flexible chain), $\lambda=7$ (close to the bicritical point) and $\lambda=15$. Here, the degree of polymerization is $N=100$. Thus the collapse transition for a flexible chain is clearly a continuous (2nd order) transition, and for a quite stiff chain it becomes a discontinuous (1st order) transition.

which D_m is an example, rather than the extrinsic metric quantities such as the density or the structure factor. It is well known and understood that the Gaussian mean-field method works quite well for intrinsic functions, while it only can give a Gaussian shape for the latter.[16] This deficiency is unavoidable in this order of the expansion in the Gibbs–Bogoliubov scheme, but it does not seriously affect either the phase structure of the system, nor any of the distributions in the chain indices, such as the amplitudes of the normal modes $\mathscr{T}_q$. The quantities $\mathscr{T}_q$ alone are sufficient to properly describe the structure of conformations and allow one to distinguish between different phases of the system. Improvements in the whole scheme, discussed in Ref. 11, can be made, but the cost in complexity is high.

Now, let us return to the discussion of the phase diagram. Curve I in Fig. 1 denotes the ordinary coil-to-globule transition for a comparatively flexible chain. This is a continuous (second order) transition[26] as may be seen from Fig. 3 (two upper curves).

If the stiffness is greater than some critical value the collapse transition (curve II in Fig. 1) becomes discontinuous (first order transition), as one can see from Fig. 3 (lower curve). The discontinuity of the coil-to-torus transition is natural since it is accompanied by a change in the spatial symmetry. It turns out that for larger $|u_2|$ the system can undergo a torus-to-spherical globule discontinuous transition (curve III in Fig. 1) restoring the spatial isotropy of the globule. Note that all curves I, II, and III intersect at a bicritical point A. Evidently, the transition III occurs when the two-body attraction exceeds the bending elasticity contribution. We shall discuss the condition of stability of the toroidal conformation in detail further in this subsection.

The distinction between various phases has been so far made by the global minimum of the free energy. We found that for the parameters in the narrow regions between the curves II′, II″ and III′, III″ the free energy possesses additional metastable minima. These boundaries of metastability are called the spinodals, and may be found from the condition of vanishing of the Hessian matrix determinant, $\det\|\partial^2\mathscr{A}/\partial X_q \partial X_{q'}\| = 0$. In other words, the spinodals correspond to the inflexion points where one of the minima disappears, and there remains only a single minimum of the free energy. In contrast, the transition curves II and III are defined by the condition that the current minimum of $\mathscr{A}$ becomes the deepest one. Observables such as the energy, $\mathscr{E}$, the radius of gyration, R_g, or the internal modes, $\mathscr{T}_q$, experience a discontinuous jump at these transition curves.

Formation of the torus during a quasistatic change of the two-body interaction from ''effective'' repulsion to attraction is illustrated in Fig. 4. Thus near the transition curve II there appear two strongly distinct geometrical parameters $D_{\max}$ and $D_{\min}$. The torus is slender is this region and becomes thicker compared to its external radius as $|u_2|$ increases. At the spinodal III″ the external and internal radii of the torus become equal and the torus ceases to exist. Let us mention also that the double squared radius of gyration by definition is bounded between these two parameters:[27] $D_{\min} \leqslant 2R_g^2 \leqslant D_{\max}$. From Tables I and II we find the following scaling laws for the parameters of the torus:

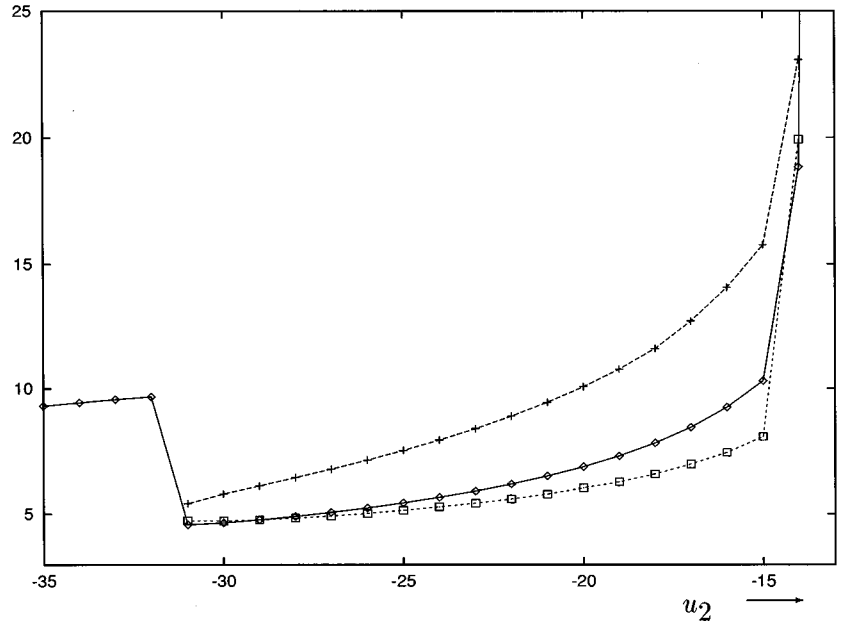

FIG. 4. Plots of the mean squared values of the external (long-dashes), $D_{\max}$, and internal (short-dashes), $D_{\min}$, diameters of the torus and of the double radius of gyration (solid line), $2R_g^2$ vs the second virial coefficient u_2. Here, the degree of polymerization is $N=100$ and the stiffness $\lambda=15$. The region $-31<u_2<-28$ corresponds to the metastable torus minimum.

$$D_{\max}\sim R^2\sim \lambda^{1/2}N^{2/3}, \tag{16}$$

$$D_{\min}\sim r^2\sim \lambda^{-1/2}N^{0.44\pm 0.02}. \tag{17}$$

It is natural that the external radius of the torus, R, scales with a positive power of the stiffness, while the internal radius, r, scales with the inverse power, so that the surface area, rR, is independent of λ. This result agrees with that of Ref. 28. The scaling, $R\sim N^{1/3}$ is also natural because it expresses the complete filling for the compact object.

The mean bending energy, $\mathscr{E}_{\text{bend}}$, depicted in Fig. 5 may be viewed as another order parameter characterizing the coil-to-torus and the torus-to-spherical globule transitions. For a quite stiff chain (upper curve) the bending energy is small in the coil state since it describes nearly a rigid rod. It increases discontinuously at the transition to the more compact toroidal globular state. Moreover, $\mathscr{E}_{\text{bend}}$ increases discontinuously again at the transition to the spherical globule. Indeed, the torus is a locally straight conformation especially optimized with respect to bending, while the spherical globule has no such special properties. The dotted lines in Fig. 5 show the values of the bending energy in the metastable minima. For example, if one goes quasistatically from the torus to the spherical globule the system will change its conformation on the spinodal III″, while for the inverse process—on the spinodal III′. Such a quasistatic process forms a hysteresis loop.

TABLE II. Values of parameters of the torus for different values of the stiffness for $u_2=-18$ and $N=100$. Here, α denotes the exponent of the appropriate power law in the stiffness parameter.

λ	10	12	15	17	20	α
$D_{\min}$	8.16	7.35	6.59	6.11	5.63	-0.52 ± 0.02
$D_{\max}$	9.44	10.48	11.61	12.34	13.75	0.53 ± 0.03

In Fig. 6 we exhibit the entropy change vs the third virial coefficient. The most striking discovery here is that there are additional toroidal phases T' and T''. They appear in a narrow region of the phase diagram around the coil-to-torus transition curve II and may be characterized as not fully compacted toroidal conformations. For higher stiffness and degree of polymerization the number of such ''exotic toroidal'' phases grows quickly, but the majority seem to be metastable. Some of them (as the phase T') may actually become stable, but in a rather narrow domain. The study of these phases is particularly difficult using numerical methods since the relaxation times around them are exceedingly long and the phases vanish even with small change of parameters. This whole aspect of the problem deserves further attention since such phases may be observable experimentally.

2. Scaling theory for the toroidal conformation

Having discussed the numerical results, we now seek to establish a simple theory of the spherical globule-to-torus transition. First, we shall try to analyze the exact solution of the self-consistent equations by extracting scalings of various terms from the numerical data. Later on, we shall try to understand those scalings in approximate analytical terms without appealing to the numerical solution.

First, the torus conformation is favorable compared to the spherical globule for the same thermodynamical parameters if the transition is accompanied by a decrease of the free energy. Thus from the standard thermodynamical principles it follows that the condition $\Delta\mathscr{A}\equiv\mathscr{A}_{\text{torus}}-\mathscr{A}_{\text{sph.gl.}}<0$

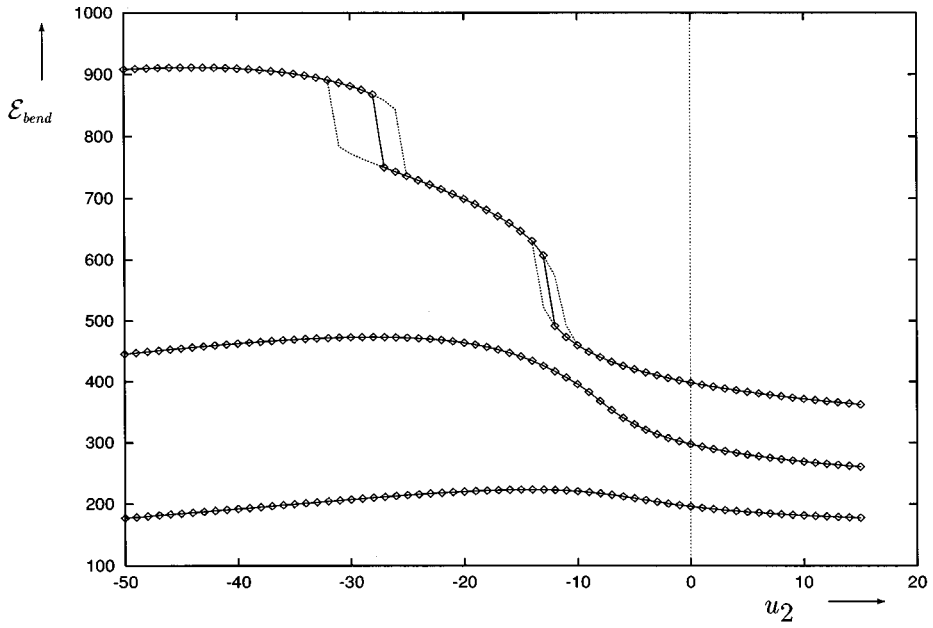

FIG. 5. Plots of the mean bending energy $\mathscr{E}_{\text{bend}}$ vs the second virial coefficient u_2 for different values of the stiffness λ (from bottom to top): 2 (slightly stiff chain), 6 (close to the bicritical point) and 15 (very stiff chain). On the upper curve the solid lines represent the value of $\mathscr{E}_{\text{bend}}$ in the global free energy minimum, whilst the dotted lines correspond to the values of $\mathscr{E}_{\text{bend}}$ in the metastable minima. These form the hysteresis loops of the first order transitions. Here, the degree of polymerization is $N=100$.

determines the region of stability of the torus, and the condition $\Delta\mathscr{A}=0$ determines the phase transition line. From the data partially presented in Tables III and IV we have obtained the following scalings for different terms in the free energy $\mathscr{A}=-T\mathscr{S}+\mathscr{E}_{\text{spring}}+\mathscr{E}_{\text{bend}}+\mathscr{E}_{\text{excl.v.}}$, by fitting around the transition line,

$$\mathscr{E}^{\text{torus}}_{\text{bend}}=A_t N^{0.9}\lambda^{0.52}, \quad \mathscr{E}^{\text{sph.gl.}}_{\text{bend}}=A_g N\lambda^{0.78}, \tag{18}$$

$$\mathscr{E}^{\text{torus}}_{\text{spring}}=B_t N^{1.22}, \quad \mathscr{E}^{\text{sph.gl.}}_{\text{spring}}=B_g N, \tag{19}$$

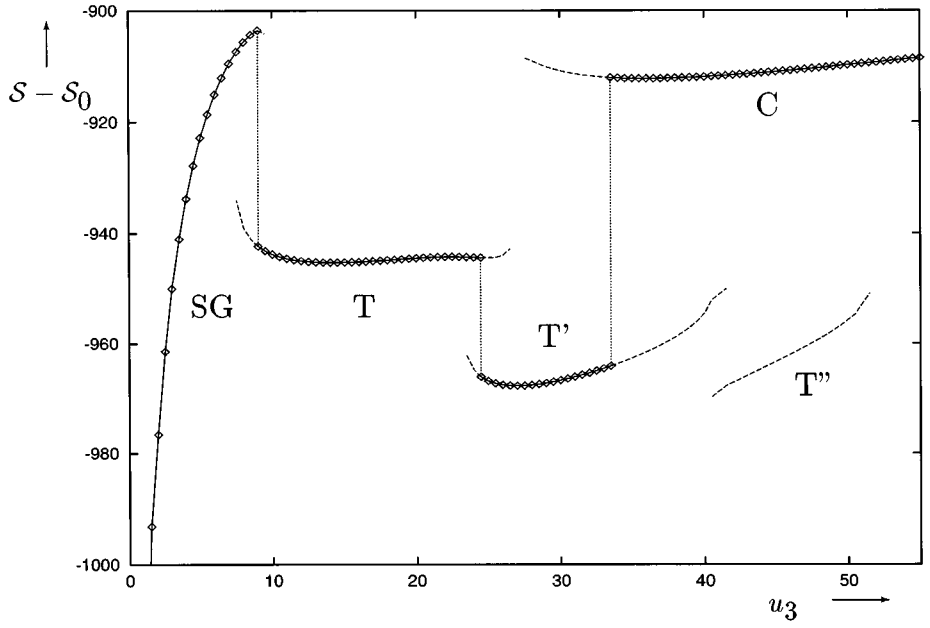

FIG. 6. Plot of the entropy $\mathscr{S}-\mathscr{S}_0$ (where $\mathscr{S}_0$ is an irrelevant normalization constant) vs the third virial coefficient u_3. Here, $u_2=-25$ and $N=100$. In this figure the solid curve with diamonds represents true equilibrium states (SG—spherical globule, T,T′—toroidal states, C—coil), the long-dashed line represents the value of the entropy in metastable states (such as a toroidal state T″) and the short-dashed vertical lines show the discontinuous transitions points.

TABLE III. Values of the bending, $\mathscr{E}_{\text{bend}}$, and spring, $\mathscr{E}_{\text{spring}}$, energies in different phases denoted in the table by superscripts: (c)—coil ($u_2=15$), (t)—torus ($u_2=-18$), (g)—spherical globule ($u_2=-40$) for different degrees of polymerization at $\lambda=15$. Here γ denotes the exponent of the appropriate power law in the degree of polymerization.

N	50	70	100	150	200	300	γ
$\mathscr{E}^{(c)}_{\text{bend}}$	188.6	256.9	362.6	540.9	719.8	1078.5	0.98±0.01
$\mathscr{E}^{(t)}_{\text{bend}}$	368.1	495.6	681.2	979.4	1267.8	1824.6	0.894±0.003
$\mathscr{E}^{(g)}_{\text{bend}}$	456.2	637.4	909.3	1362.5	1815.8	2723.0	0.997±0.001
$\mathscr{E}^{(c)}_{\text{spring}}$	157.5	227.1	329.0	496.6	663.6	996.8	1.03±0.02
$\mathscr{E}^{(t)}_{\text{spring}}$	43.28	66.15	102.8	168.3	238.2	387.5	1.22±0.01
$\mathscr{E}^{(g)}_{\text{spring}}$	22.95	32.45	46.65	70.42	93.92	140.4	1.01±0.01

$$\mathscr{E}^{\text{torus}}_{\text{excl.v.}}=-C_t\frac{|u_2|^2}{u_3}N,\quad \mathscr{E}^{\text{sph.gl.}}_{\text{excl.v.}}=-C_g\frac{|u_2|^2}{u_3}N, \tag{20}$$

$$\mathscr{S}^{\text{torus}}=s_0N-D_tN^{1.22},\quad \mathscr{S}^{\text{sph.gl.}}=s_0N, \tag{21}$$

where $A_t\simeq 2.767$, $A_g\simeq 1.104$, $B_t\simeq 0.367$, $B_g\simeq 0.468$, $C_g>C_t$ and $D_t\simeq 0.18$ in the range of parameters: $-50\leqslant u_2\leqslant -20$, $2\leqslant u_3\leqslant 10$ and $10\leqslant\lambda\leqslant 20$, $50\leqslant N\leqslant 300$. Here, we have only kept strong dependencies and specified only those numerical constants that are relevant for our analysis. These scaling have been obtained separately for the globule and the torus, and to find the region of stability of the torus one has to extrapolate $\mathscr{A}^{\text{sph.gl.}}$ to the torus region and compare it with $\mathscr{A}^{\text{torus}}$ for the same values of thermodynamical parameters. Note also that most of the above scalings are well known for the spherical globule phase[11,29] and can be obtained from Eq. (26) below. As to the scalings for the torus, they are more nontrivial.

Thus we obtain the stability condition

$$\frac{|u_2|}{u_3^{1/2}}<\sqrt{\frac{A_g\lambda^{0.78}+B_g-A_t\lambda^{0.52}N^{-0.1}-(B_t-D_t)N^{0.22}}{C_g-C_t}}. \tag{22}$$

One can see that for a given N there exists a minimal stiffness, λ_c, that results in a torus, and it can be determined by requiring that the numerator inside the square root in Eq. (22) vanishes. For very stiff polymers the first term in the square root dominates and the torus exists if,

$$\frac{|u_2|}{u_3^{1/2}}<\lambda^{0.39\pm 0.01}. \tag{23}$$

Now, for a fixed stiffness the torus is possible between the maximal, $N_{\max}$ and minimal, $N_{\min}$, chain lengths that are determined by positivity of the numerator in Eq. (22), which is opposed by the third and fourth terms. Let us mention that values of the critical stiffness (that is close to the stiffness in the bicritical point), λ_c, obtained from Eq. (22) are in good agreement with the exact results for the chain lengths considered in the paper. Finally, the function $\lambda_c(N)$ is decreasing with N up to approximately the degree of polymerization $N_c\simeq 3\cdot 10^3$ and then grows as $\lambda_c\sim N^{0.28}$. Thus for quite long chains the region of the torus phase moves to the right and narrows down. The latter conclusion is currently difficult to check by direct numerical analysis due to the large degrees of polymerization required, but it does agree qualitatively with the predictions of Ref. 28. We believe also that this prediction should be quite robust to different models, and would encourage experimental study of the matter.

To understand the main qualitative properties of the equilibrium theory we consider the equation for the effective potential (2). For small q, we can seek solution using the *Ansatz*,[29]

$$\Delta V_q=NA^{-1}\mathbf{q}^{2\beta},\quad \mathbf{q}\equiv\frac{2\pi q}{N}, \tag{24}$$

where A is some, as yet unknown, constant. If we define parameters b and ν by the relation

$$D_{nn'}\simeq b^2|n-n'|^{2\nu}, \tag{25}$$

then $\nu=\beta-1/2$ and $b\simeq\sqrt{Ak_BT}$. Therefore, for small $\mathbf{q}$ Eq. (2) reduces to the dominant balance equation,

$$\frac{k_BT}{l^2}\left(\mathbf{q}^2+\frac{\lambda}{l}\mathbf{q}^4\right)-\frac{k_BT}{b^2}\mathbf{q}^{2\nu+1}=I'u_2b^{-5}\mathbf{q}^{5\nu-1}+I''u_3b^{-8}\mathbf{q}^{8\nu-2}. \tag{26}$$

TABLE IV. Values of the bending, $\mathscr{E}_{\text{bend}}$, and spring, $\mathscr{E}_{\text{spring}}$, energies in different phases denoted in the table by superscripts: (c)—coil ($u_2=15$), (t)—torus ($u_2=-18$), (g)—spherical globule ($u_2=-40$) for different values of stiffness at $N=100$. Here, α denotes the exponent of the appropriate power law in the stiffness parameter.

λ	02	05	10	12	15	20	24	α
$\mathscr{E}^{(c)}_{\text{bend}}$	177.5	244.1	312.8	334.2	362.6	402.2	429.8	0.35±0.01
$\mathscr{E}^{(t)}_{\text{bend}}$			564.9	611.6	681.2	781.3	899.3	0.52±0.05
$\mathscr{E}^{(g)}_{\text{bend}}$	192.0	401.8	679.1	775.5	909.3	1116.8	1279.1	0.78±0.02
$\mathscr{E}^{(c)}_{\text{spring}}$	252.0	270.0	302.1	313.4	329.0	352.5	369.5	
$\mathscr{E}^{(t)}_{\text{spring}}$			93.60	98.70	102.8	107.9	104.7	
$\mathscr{E}^{(g)}_{\text{spring}}$	53.55	49.95	47.70	47.25	46.65	46.20	45.15	

Here I', I'' are some irrelevant numerical constants and the third term represents the entropic contribution. We may extract different regimes depending on the parameters. If $u_2>0$ and λ is small, we find dominant balance between the q^2 and the u_2 term, which gives the Flory exponent $\nu=3/5$ and $b^2\sim(u_2 l^2)^{2/5}$. Similarly for very large stiffness we obtain the rigid rod exponent $\nu=1$ and $b^2\sim(u_2 l^3/\lambda)^{2/5}$. When $u_2=0$ we have a balance between $\mathbf{q}^2$ and the u_3 term, and we get the Θ point: $\nu=1/2$, $b^2\sim(u_3 l^2)^{1/4}$. If $u_2<0$ and λ is small, we are in the spherical globule state with balance between the two-body and three-body terms giving $\nu=1/3$ and

$$b^2\sim(u_3/|u_2|)^{2/3}. \tag{27}$$

Note that one cannot use the same estimates for the torus state because the amplitudes of the Fourier modes are more complicated [see Fig. 2(b)]. These may be approximated by the Lorentzian form, $\mathscr{T}_q\sim(A-B\mathbf{q}^2+\mathbf{q}^4)^{-\beta/2}$, rather than a simple power law. Obviously, when the bending energy contribution exceeds the excluded volume interaction the above balance, necessary for the spherical globule, breaks down. Thus such a globule ceases to exist and, as we know, becomes a torus. This yields the condition, $\lambda>u_2 b^{-5}$, or

$$\frac{|u_2|}{u_3^{5/8}}<\lambda^{3/8}, \tag{28}$$

which qualitatively agrees with our phenomenological estimate far from the critical point (23).

B. Kinetics

In this subsection we shall consider kinetics determined by Eq. (5) after an abrupt quench $u_2^i\to u_2^f$, with a fixed stiffness λ, from one phase to another in the phase diagram of Fig. 1. Note that modest adaptations permit us to incorporate the hydrodynamic effect. We have illustrated the method for kinetics of a flexible homopolymer in a previous work in Ref. 11, and shall therefore not dwell much on the topic here.

1. Coil–torus–spherical globule kinetics

To start with, let us briefly recall the results for kinetics at the coil-to-globule transition of a flexible polymer ($\lambda=0$) discussed in detail in Refs. 10 and 11. The early stage of that kinetics is governed by the process of the spinodal decomposition in the internal metric of the chain, that is formation of a quasiperiodic array of locally collapsed clusters along the chain. This corresponds to an exponentially fast decrease of the high-q Fourier modes, $\mathscr{T}_q(t)$, while the low-q modes change relatively slowly. The duration of the spinodal regime is rather short and almost independent of the system size. Gradually the kinetics enters the coarsening stage, which on the contrary is governed by decrease of the low-q modes (large distances along the chain) with high-q modes starting to grow slowly. The characteristic time scale of the middle kinetic stage, τ_m, is defined as the moment when the second mode $\mathscr{T}_2(t)$ reaches its minimum, and we found that it scales as $\tau_m\sim N^2$ without hydrodynamics. The final stage is described by an exponential relaxation of the Fourier modes towards the final equilibrium state corresponding to the new minimum of the free energy. Thus according to the kinetic equation (5) the motion in the phase space of variables $\mathbf{X}$ proceeds along the pathway first in the directions of the high-q components, then turns around and continues in the low-q directions, finally reaching the minimum of $\mathscr{A}$ along the first axis X_1.

TABLE V. Values of the characteristic duration of the second kinetic stage, τ_m, for different values of the degree of polymerization N and the stiffness parameter λ. The initial and final values of the second virial coefficient are 15 and -25, respectively.

N	30	50	70	100	150	200	300
$\tau_m(\lambda=0)$	1.8	4.4	8.3	16.6	38	70	156
$\tau_m(\lambda=2)$	3.85	9.05	15.3	27.0	53	90	200
$\tau_m(\lambda=4)$	5.22	13.4	22.4	38.1	71	114	234
$\tau_m(\lambda=6)$	6.30	17.6	30.5	51.8	94	146	280

Let us consider now the kinetics for a similar quench at a relatively small stiffness $\lambda<\lambda_c$, where the equilibrium collapse transition (curve I in Fig. 1) is still second order. The kinetics remains qualitatively the same, but it takes longer and the spinodal decomposition effect becomes weaker with increasing stiffness. In Table V we present the values of the time scale of the middle stage τ_m for different values of the stiffness and the degree of polymerization. It may be estimated as,

$$\tau_m(\lambda)\sim\tau_m^{\mathrm{flex}}+a\lambda^{1.2\pm0.1}N^{1.3\pm0.2}. \tag{29}$$

Thus for a fixed λ this time becomes close to that of a flexible homopolymer ($\tau_{in}^{\mathrm{flex}}\sim N^2|u_2|^{-2}$, see Ref. 11) for very long chain lengths, being a crossover between N^2 and a weaker power of N for smaller sizes.

The situation changes dramatically after the bicritical point λ_c. Consider quenches along the path C–T–G further away from the point A in Fig. 1. In Fig. 7 the time evolution of the mean squared radius of gyration for quenches with different final second virial coefficients are depicted. One observation is that the kinetics of a stiff polymer is considerably longer than of a flexible polymer (solid curve). Another observation from Fig. 7 and particularly from Fig. 8, where we present the time evolution of the mean energy of the system, is that the kinetic process has several slow and fast regimes. Their duration and even number depends strongly on the quench depth. A better quantity to describe the rate of kinetics is $-d\mathscr{A}/dt$ and by Eq. (7) it is related to the modulus of the free energy gradient. This is drawn in Fig. 9 for the same quenches as in the two previous figures.

Since the kinetics in Eq. (5) is simply the motion against the free energy gradient, in Fig. 10 we schematically illustrate the free energy profiles for different values of u_2. Let us emphasize here that the torus minimum lies farther from the initial coil minimum than the spherical globule one. This has been established from the careful analysis of various observables for different kinetic regimes. To explain this property one may argue that the spherical globule minimum may be obtained by a continuous deformation of the coil minimum, what corresponds to the second order of the coil-to-spherical globule transition (curve I in the phase diagram), whereas the

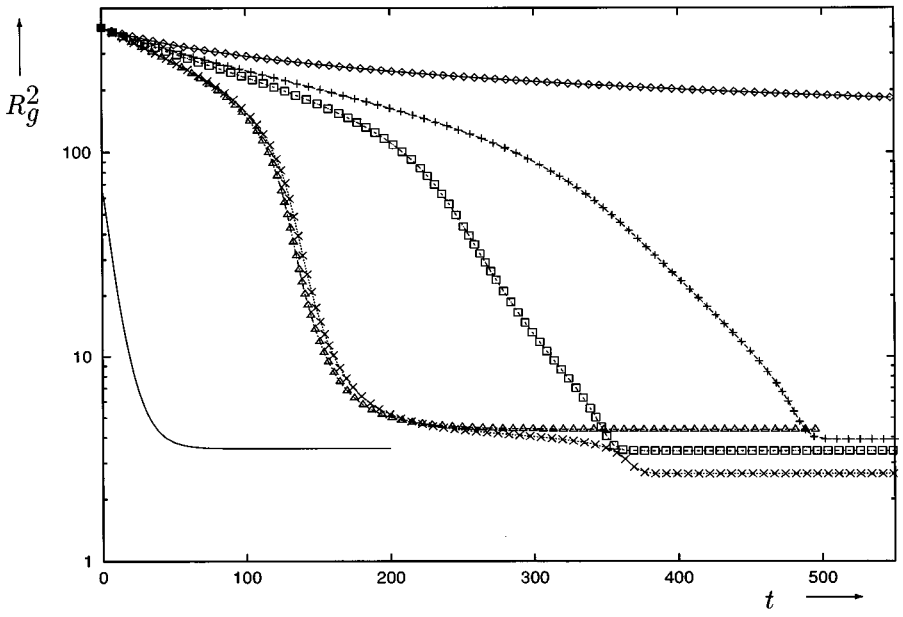

FIG. 7. Time evolution of the mean squared radius of gyration R_g^2 for $N=100$, $\lambda=15$ for different quenches from the coil state along the path C–T–G in Fig. 1 (from top to bottom): diamonds—$u_2=-12$ (quench inside the coil state), pluses—$u_2=-18$ (quench to the torus state just beyond the spinodal II″), quadrangles—$u_2=-20$ (quench deep to the torus state), crosses—$u_2=-25.6$ (quench to the torus state just above the spinodal III′) and triangles—$u_2=-26$ (quench to the metastable region between the curves III′ and III″). The solid line corresponds to the flexible chain $\lambda=0$, and to the quench to $u_2=-25$ (globule).

torus is a topologically different conformation and may be obtained from the coil by a first order transition (curve II).

Thus, we start at the point A in Fig. 10, which is the unique free energy minimum for the coil. After an instantaneous quench the initial profile is transformed and the system happens to be in a point along the arrow A–E. The resulting kinetics depends on the free energy profile for appropriate final value of u_2. Diamonds in Figs. 7–9 describe the quench coil-to-coil, with the $\mathscr{A}$ profile only slightly deformed. Such a kinetics therefore is given by a monotonic relaxation. For

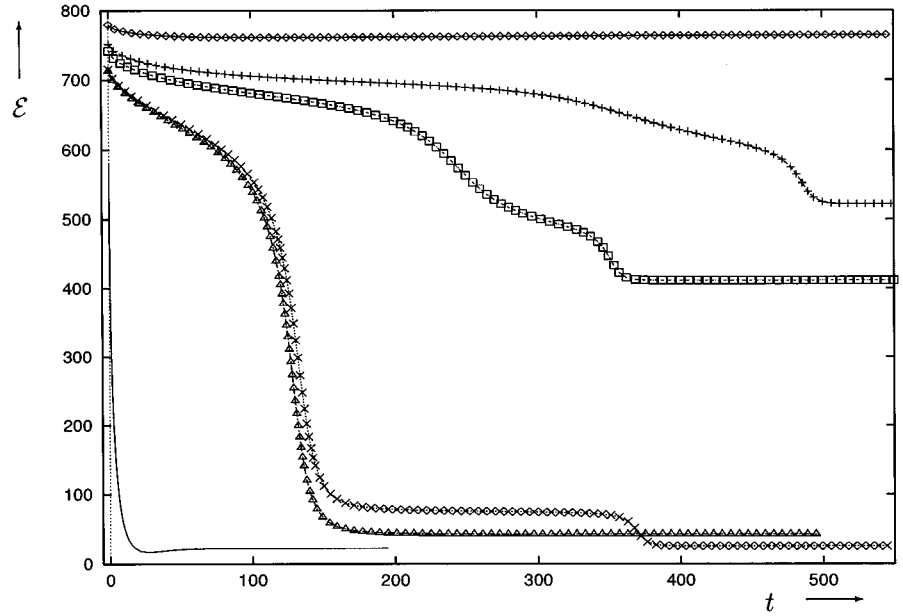

FIG. 8. Time evolution of the mean energy $\mathscr{E}$ for the same parameters and quenches as in Fig. 6. We preserve the same notations for the lines and points, but the solid line is drawn rescaled: $500+\mathscr{E}/2$ for convenience.

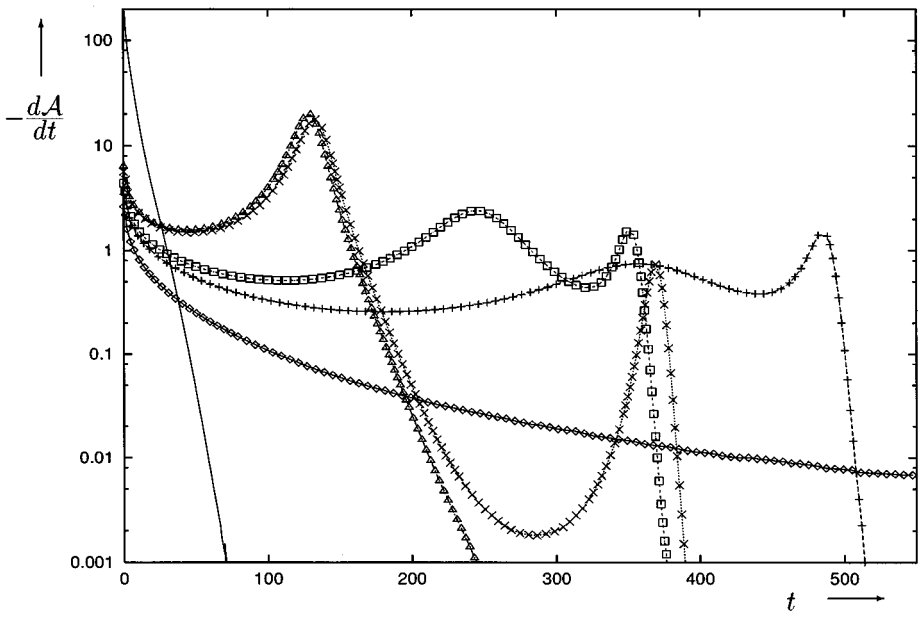

FIG. 9. Time evolution of minus time derivative of the ensemble averaged free energy $-d\mathcal{A}/dt$ for the same parameters and quenches as in Fig. 6.

quenches from the coil to the region between curves II and II″ in Fig. 1 the kinetics leads to the metastable coil final state.

Pluses in Figs. 7–9 designate the kinetics for a quench of type A–B in Fig. 10, for which the torus is the unique free energy minimum. So after a long slow regime, during which the coil uniformly contracts, it undergoes a rapid final restructuring during a short time forming the torus. We shall return to the question of this transformation later. Quadrangles denote a similar kinetic process, but in the region of the dynamical variables **X** near the place where the spherical globule minimum will further emerge. Here, the free energy first becomes steeper and then flattens. This leads to a kinetic acceleration (the first peak in Fig. 9) and consequent slowing down.

Crosses in Figs. 7–9 correspond to the quench A–C,

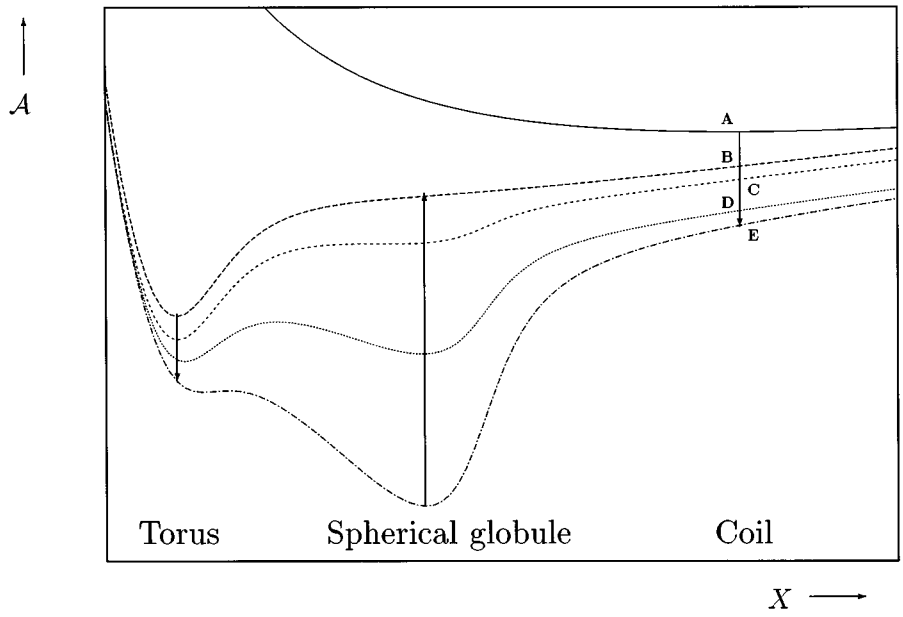

FIG. 10. Schematical profiles of the free energy $\mathcal{A}$ parametrized by the dynamical variables **X** for different values of the second virial coefficient u_2. The system is quenched from the point A (which corresponds to the global free energy minimum for the extended coil) along the arrow to points: B (quench to the torus state), C (the same with a kinetic slowing down), D (quench to the metastable spherical globule state), E (quench to the stable spherical globule state). Long and short arrows correspond to quenches from the spherical globule and torus.

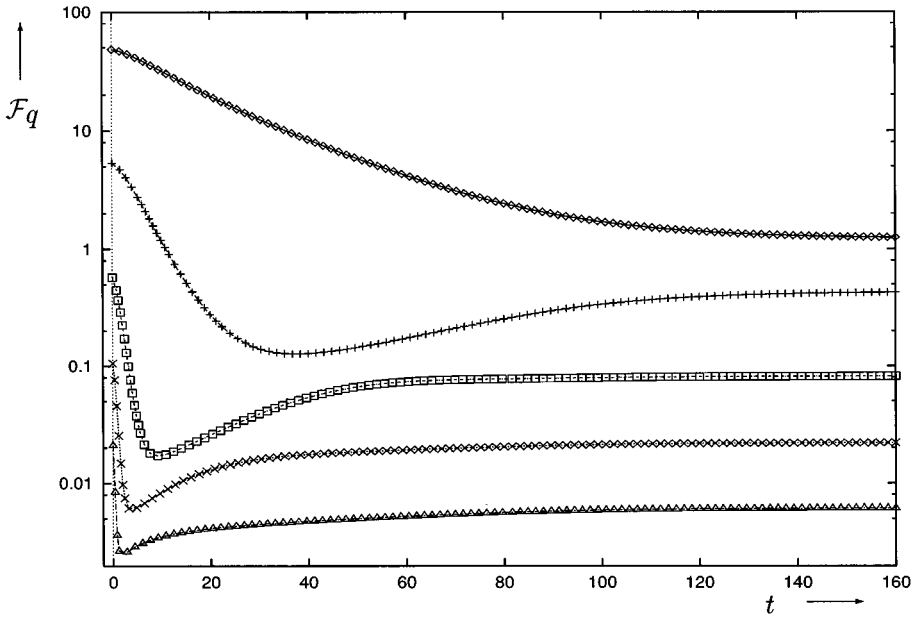

FIG. 11. Time evolution of the Fourier modes $\mathcal{F}_q$ for $q=1,2,5,10,20$ (from top to bottom) for flexible chain $\lambda=0$. Here, $N=150$, the initial and final values of the second virial coefficients are 15 and -25, respectively.

where the unstable spherical globule is clearly manifested. The slow regime between the first and the second peaks in Fig. 9 can be made arbitrarily long by approaching the spinodal III′ from above in the phase diagram. Once we have crossed that spinodal (triangles in Figs. 7–9 and profile D in Fig. 10), there appears the metastable spherical globule minimum. Thus the kinetics stops when the system is trapped in that minimum. This minimum becomes global after the critical curve III and unique after the spinodal III″ in Fig. 1. Obviously, the kinetics for such quenches remains qualitatively the same as for quench A–D.

To understand the conformational changes during kinetics one has to appeal to more detailed characteristics such as the Fourier modes $\mathcal{F}_q$. In Fig. 11 we show the time dependencies of these for a flexible chain ($\lambda=0$) and in Figs. 12 and 13 for a stiff chain and quenches A–E (to the spherical

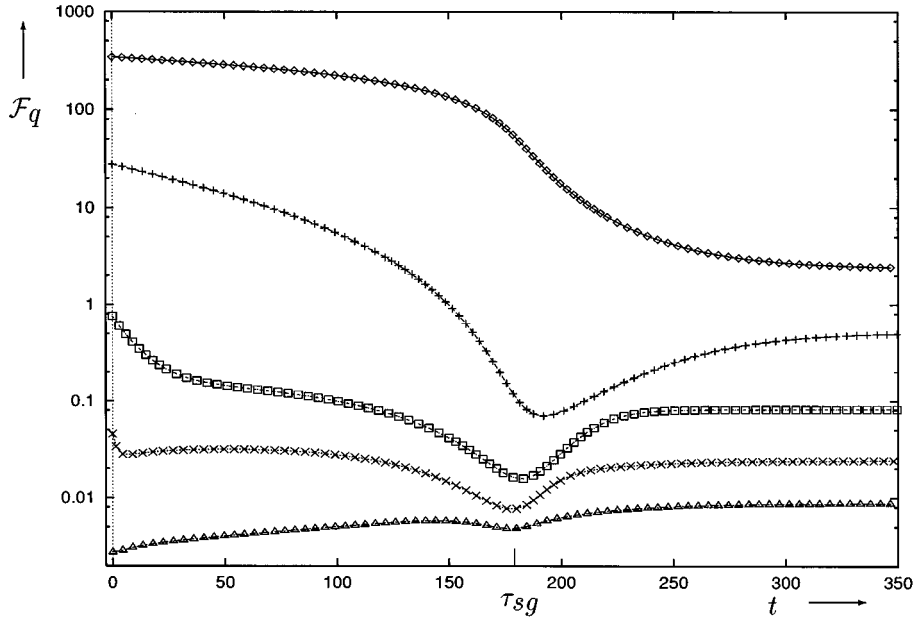

FIG. 12. Time evolution of the Fourier modes $\mathcal{F}_q$ for $q=1,2,5,10,20$ (from top to bottom) for a stiff chain $\lambda=15$. Here, $N=150$, the initial and final values of the second virial coefficients are 15 and -30 (quench to the spherical globule phase), respectively.

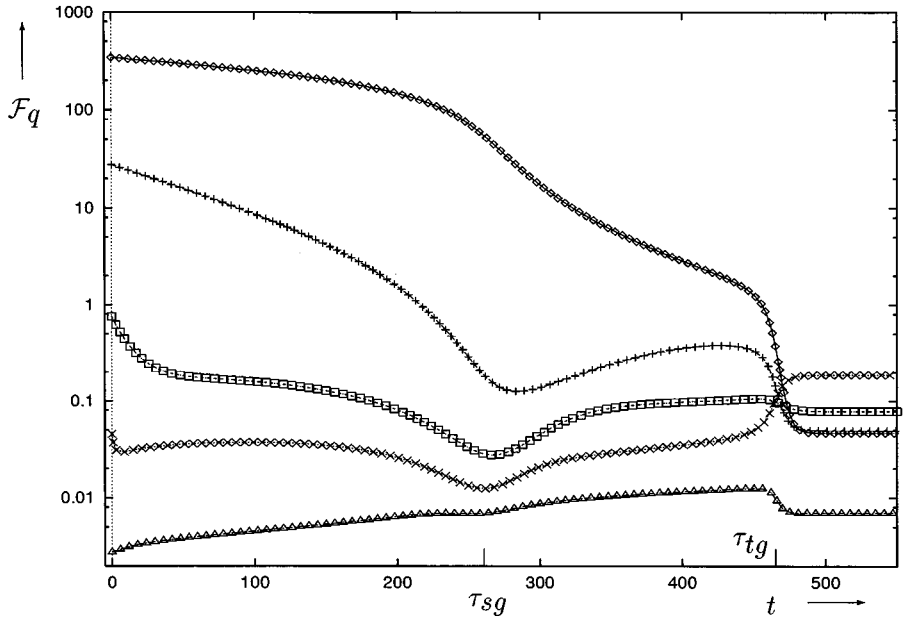

FIG. 13. Time evolution of the Fourier modes $\mathcal{F}_q$ for $q=1,2,5,10,20$ (from top to bottom) for a stiff chain $\lambda=15$. Here, $N=150$, the initial and final values of the second virial coefficients are 15 and -25 (quench to the torus phase), respectively.

globule) and A–C (to the torus slightly above the spinodal III′), respectively. From Fig. 11 the above mentioned spinodal decomposition in the internal metric of the chain can be seen for small t. It is absent in Figs. 12 and 13, where the high-q modes increase slowly in contrast to the exponential decrease for some chain indices characteristic for the spinodal decomposition. Indeed, stiffness of the chain does not permit formation of locally collapsed clusters, and kinetics proceeds by a uniform shrinking of the whole chain. The process accelerates at about time τ_{sg}, corresponding to the first peak for triangles and crosses in Fig. 9. Around the time τ_{sg} low-q modes (except the first, which is monotonically decreasing) reach their minimum. This time tends to the time τ_m for a flexible chain as $\lambda\to 0$, which, however, being the minimum of only $\mathcal{F}_2$, does not correspond to any special behavior of the free energy, radius of gyration or any other observable at this moment. Collapse of a stiff chain is impeded because bending is unfavorable and the chain prefers to be locally straight. However, when the collapsing chain becomes sufficiently compact, the two-body attraction overcomes that tendency and the system undergoes a rapid final shrinking in a highly collective way accompanied by strong mode coupling. We emphasize that this is a typical effect of frustration caused by the competition of stiffness and the excluded volume forces. Similar collective phenomenon in kinetics appeared for instance in our study of the phase separation of periodic heteropolymers.[16] For the quenches to the spherical globule phase (see Fig. 12) after that abrupt shrinking there remains only a slow relaxational stage approaching the final equilibrium.

When the system has been quenched to the torus phase (Fig. 13) the collapse slows down for some time after τ_{sg} until at the moment τ_{tg}, there appears a new kinetic stage. Here, again we have a collective mode coupling phenomenon, which in fact corresponds to the transformation of a spherical globulelike state to the toroidal conformation. Indeed, let us compare $\mathcal{F}_q$ for the torus and the spherical globule in Fig. 2(b). The main difference is that, for the former, the $\mathcal{F}_q$ are greater than for the latter only in some intermediate q range, being smaller otherwise. Thus in Fig. 13, around the time τ_{tg} the modes number $q=1$, 2, and 20 experience significant decrease, but for $q=10$ a significant increase and $\mathcal{F}_5$ changes a little bit. Note that the final relaxational stage for the torus is the fastest one compared to the spherical globule or coil.

Hence there are two discernible characteristic times τ_{sg} and τ_{tg} in the collapse kinetics. Prior to the spinodal II″ the time derivative of the free energy in Fig. 9 possesses only a single peak. Its position in time determines the first time τ_{sg}, which may be interpreted as the time necessary for the unstable coil to become the torus (curve B in Fig. 10). As one can see from Fig. 14 this time diverges on approaching the spinodal II″ (from below), and it may be approximated with a good precision in its close vicinity by the power law,

$$\tau_{tg}^{\mathrm{II}''-} \simeq \tau_0^{\mathrm{II}''-} + A^{\mathrm{II}''-}(u_2^{\mathrm{II}''} - u_2)^{-\delta^{\mathrm{II}''-}}. \tag{30}$$

In Table VI we present the parameters of the law (30) obtained by fitting. The critical exponent is equal to $\delta^{\mathrm{II}''-} \simeq 3/2 \pm 0.1$ and the prefactor scales $A^{\mathrm{II}''-} \sim N^2$ (or more exactly the power is 1.97 ± 0.08). Note that τ_{tg} diverges again near the spinodal III′, but we shall present the appropriate scaling law later on.

For quenches farther to the region between curves II″ and III′ there appears a new maximum in $-d\mathcal{A}/dt$ laying earlier in time (see Fig. 9). It determines the moment, τ_{sg},

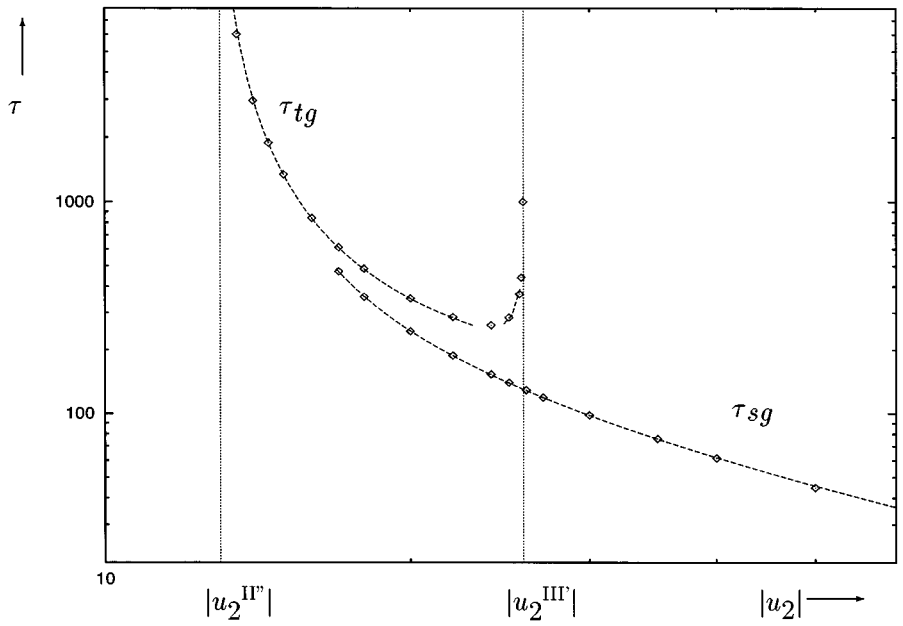

FIG. 14. Plots of the characteristic collapse times τ_{sg} and τ_{tg} vs modulus of the second virial coefficient $|u_2|$. Points have been obtained from the numerical data and the long-dashed lines represent the fitted theoretical dependencies according to the laws (Refs. 30, 31, 34). The short-dashed vertical lines denote the spinodals II″ and III′. These results are for $N=100$ and $\lambda=15$.

which is the time for the unstable coil to become unstable (and later after III′ stable) spherical globule. This time for sufficiently large $|u_2|$ may be approximated by the law,

$$\tau_{sg} \simeq A^{sg}(u_2^{sg}-u_2)^{-\delta^{sg}}, \tag{31}$$

where u_2^{sg} may be interpreted as continuation of the curve I in the phase diagram. The parameters obtained from the fitting are presented in Table VI. The exponent is $\delta^{sg}\simeq 1$ and the prefactor scales as $A^{sg}\sim N^{1.6\pm 0.16}$. These exponents are probably in some cross-over regime. Nevertheless, from Fig. 14 it seems that τ_{sg} is well described by such a power law.

2. Kinetics between the torus and spherical globule phases

In Fig. 15 we present the time evolution of the mean squared radius of gyration during kinetics from the toroidal state (point T in Fig. 1) to the spherical globule (around point G in Fig. 1). This can be understood from the sketch of the free energy profile in Fig. 10. Thus we start from the torus minimum on the curve marked B and quench vertically down to the curve E. Since we have instantaneously increased the two-body attraction the torus undergoes a rapid shrinking (displayed in Fig. 15) preserving its shape. Then there follows a slow stage, which can be made very long by approaching the spinodal III″ from below (this corresponds to the sequence of plots from triangles to pulses in Fig. 15). After the slow regime there is an abrupt collective transformation of the torus to the globule, and then a slow exponential optimization of the surface area. Once the quench is done above the spinodal III″, the system remains in the metastable torus (diamonds in Fig. 15).

TABLE VI. Values of the parameters, τ_0, A, u_2^c, and δ, in the characteristic kinetic time law (Refs. 30, 31) for the times τ_{sg} and τ_{tg} is the folding kinetics.

N	70	100	150	200	300
			τ_{tg}		
$\tau_0^{\mathrm{II}''_-}$	86	123	193	339	623
$A^{\mathrm{II}''_-}$	1832	3569	7705	15500	30830
$-u_2^{\mathrm{II}''}$	12.87	12.84	12.82	12.69	12.75
$\delta^{\mathrm{II}''_-}$	1.47	1.40	1.40	1.51	1.56
			τ_{sg}		
A^{sg}	674	1335	2720	4224	6794
$-u_2^{sg}$	13.83	13.97	14.14	14.30	14.60
δ^{sg}	0.92	0.94	0.99	1.01	1.04

Accordingly, one can define the characteristic time of the unstable torus to the spherical globule transformation, $\tau_{t\to s}$, which below and near the spinodal III″ diverges as a power law,

$$\tau_{t\to s} \simeq \tau_0^{t\to s} + A^{t\to s}(u_2^{\mathrm{III}''}-u_2)^{-\delta^{\mathrm{III}''_-}}, \tag{32}$$

where $\delta^{\mathrm{III}''_-} = 1/2 \pm 0.06$ and $A^{t\to s}$ slightly depends on the system size for large N as one can see from Table VII.

Similarly, in Fig. 16 we study the inverse process describing the kinetics of the globule-to-torus transformation (see the arrow from the curve E to B in the sketch Fig. 10). The first stage is a fast uniform expansion of the globule due to that the attractive force has diminished. The rest of this kinetics is reminiscent to the part of the coil-to-torus kinetics after the quench A–B in Fig. 10 starting from the head of the long arrow. Approaching the spinodal III′ from above makes the slowing down very long, and the globule turns into the

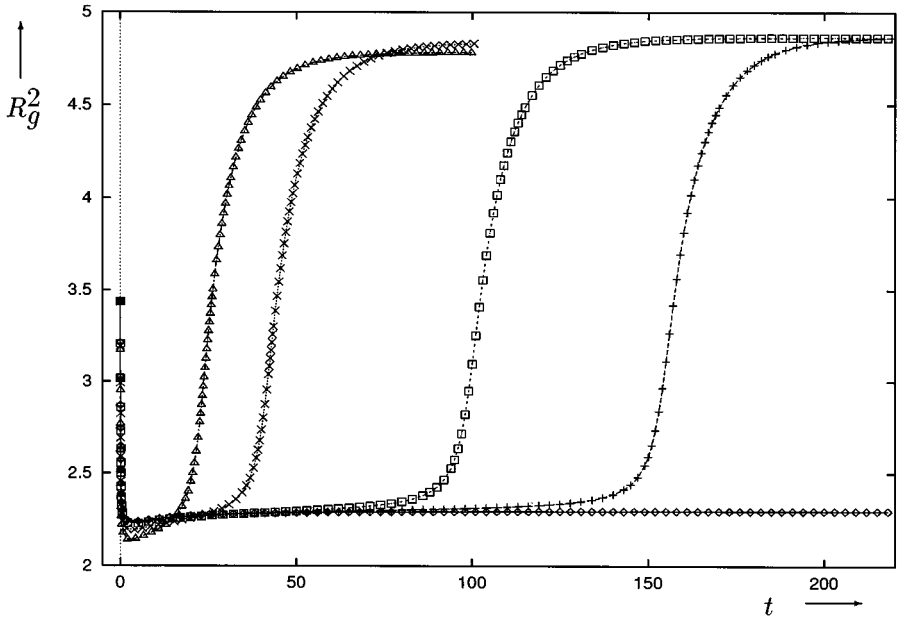

FIG. 15. Time evolution of the mean squared radius of gyration R_g^2 for $N=100$, $\lambda=15$ for different quenches from the torus state (point T on the phase diagram in Fig. 1) along the path T–G: triangles—$u_2=-33$ (quench deep to the spherical globule state), crosses—$u_2=-32$, quadrangles—$u_2=-31.4$, pluses—$u_2=-31.3$ (quench to the spherical globule state just beyond the spinodal III″) and diamonds—$u_2=-31.2$ (quench to the metastable region between the curves III′ and III″).

torus quickly in a collective fashion described above (see Fig. 13). Analogously, quenches below the spinodal III′ leave the system in the metastable spherical globule. Behavior of the free energy for these kinetic processes is consistent with the changes of R_g^2.

Analogously, the characteristic time of the unstable spherical globule to the torus transformation, $\tau_{s\to t}$, diverges as a power law above and near the spinodal III′,

$$\tau_{s\to t}\simeq\tau_0^{s\to t}+A^{s\to t}(u_2-u_2^{\mathrm{III}'})^{-\delta^{\mathrm{III}''}_{+}}, \tag{33}$$

where $\delta^{\mathrm{III}'}_{+}=1/2\pm0.05$ and the prefactor scales approximately as N: $A^{s\to t}\sim N^{1.12\pm0.04}$. The time τ_{tg} for collapse kinetics near the spinodal III′ behaves in a similar manner as $\tau_{s\to t}$ since it describes here the same process, and roughly,

$$\tau_{tg}\simeq\tau_{sg}+\tau_{s\to t}. \tag{34}$$

TABLE VII. Values of the parameters, τ_0, A and u_2^c in the kinetic laws (Refs. 32, 33) for the kinetics between different globular states.

N	70	100	150	200
	Spherical globule→Torus			
$\tau_0^{s\to t}$	−25.9	−28.0	−51.0	−71.6
$A^{s\to t}$	77.6	89.5	137.6	194.5
$-u_2^{\mathrm{III}''_-}$	24.40	25.81	26.82	27.32
	Torus→Spherical globule			
$\tau_0^{t\to s}$	−23.5	−13.1	−11.1	−11.7
$A^{t\to s}$	61.4	48.3	44.0	42.7
$-u_2^{\mathrm{III}'_-}$	25.38	31.22	40.89	50.09

3. Unfolding kinetics of a globular state to the coil

The time evolution of R_g^2 during the inverse kinetics (quench to the coil) is exhibited in Fig. 17. For a flexible homopolymer (solid line) it grows quickly for early times and exponentially tends to the final extended state. The unfolding kinetics takes much longer than the corresponding folding kinetics. The appropriate internal modes are presented in Fig. 18. First all modes undergo quick growth, which, however, as opposed to the spinodal kinetic stage of the folding is not exponential, but describes a uniform expansion of the globule. Further the first mode continues to increase, while all other modes reach their maximum and start to decrease slightly. Analogously to the collapse kinetics (see Ref. 11 for more detail) one may introduce the characteristic unfolding time τ_m^u, as the moment of maximum of $\mathscr{T}_2(t)$, the ''total'' unfolding time, $\tau_t^u[R_g^2(\tau_t^u)=0.99R_g^2(\infty)]$, and the time of the final relaxation to the extended coil, τ_f^u $[R_g^2(t)=R_g^2(\infty)-\mathrm{const}\exp(-t/\tau_f^u)]$. These times are exhibited in Table VIII. It seems that the time τ_m^u scales with a somewhat higher power of N than the collapse kinetics, that is $\tau_m\sim N^2$. As for the times $\tau_{f,t}^u$ they should scale with the exponent $\gamma=2\nu_F+1$, where $\nu_F=3/5$ is the Flory swelling exponent. However, due to the deficiency of the Gaussian approximation discussed in note 24, we obtain a higher estimate for γ unless special measures have been taken.

For a stiff chain the unfolding kinetics is similar for both the spherical globule and torus initial states. This is roughly illustrated by the sketch in Fig. 10, where the unfolding kinetics corresponds to the rolling downhill the curve A. In Fig. 19 we show the conformational change in terms of D_m

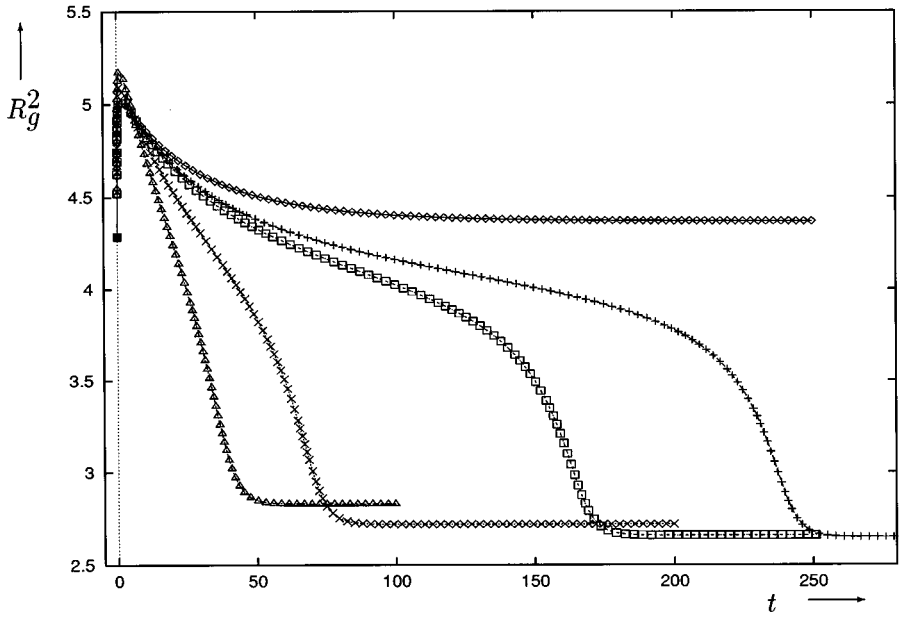

FIG. 16. Time evolution of the mean squared radius of gyration R_g^2 for $N=100$, $\lambda=15$ for different quenches from the spherical globule state (point G on the phase diagram in Fig. 1) along the path G–T: triangles—$u_2=-24$ (quench deep to the torus state), crosses—$u_2=-25$, quadrangles—$u_2=-25.6$, pluses—$u_2=-25.7$ (quench to the torus state just above the spinodal III″) and diamonds—$u_2=-26$ (quench to the metastable region between the curves III′ and III″).

during the spherical globule-to-coil kinetics. First the globule swells, then it forms an intermediate nonequilibrium torus, which finally opens up and expands. It is interesting to stress that such torus is related to one of the semidense torii states discussed earlier in the equilibrium subsection. The unfolding kinetics turns out to be sensitive to these intermediate torii. For instance, in Fig. 17 the kinetics for curve denoted by quadrangles is trapped in one such metastable states. The topography of the free energy is rather craggy around the spinodal II′, and there are also spinodals associated with other torii states. For this reason it is hard to extract the value of the critical exponent $\delta^{\mathrm{II}'}_{+}$ in a scaling law similar to Eq. (32), although the effects of slowing down near the spinodal

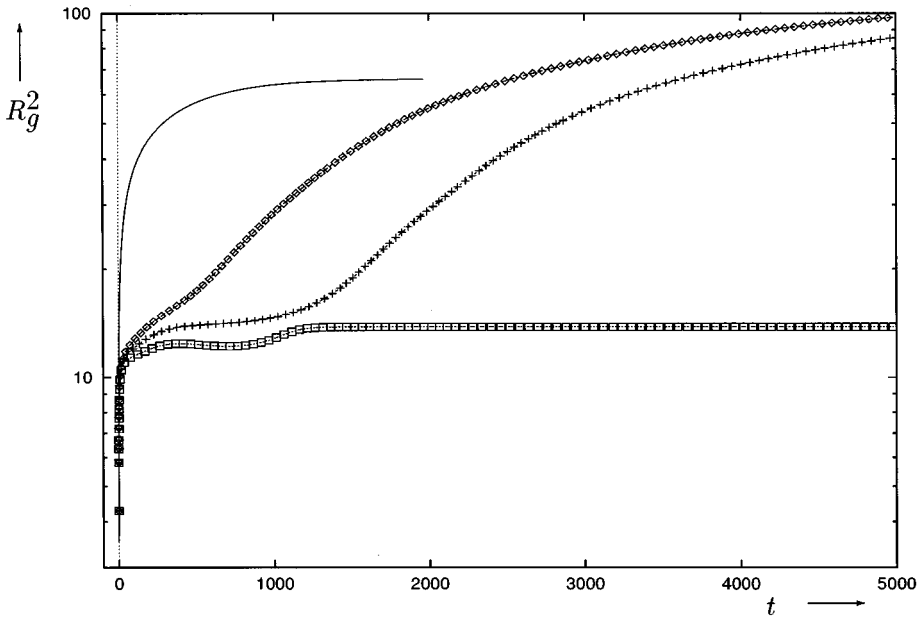

FIG. 17. Time evolution of the mean squared radius of gyration R_g^2 for $N=100$, $\lambda=15$ for different quenches from the spherical globule state (point G on the phase diagram in Fig. 1) along the path G–T–C: diamonds—$u_2=-11.7$ (quench deep to the coil state), pluses—$u_2=-11.8$ (quench just beyond spinodal II′), and quadrangles—$u_2=-11.9$ (quench to the metastable torus region between curves II′ and II″). The solid line corresponds to the kinetics of a flexible chain $\lambda=0$, with the quench to $u_2=15$.

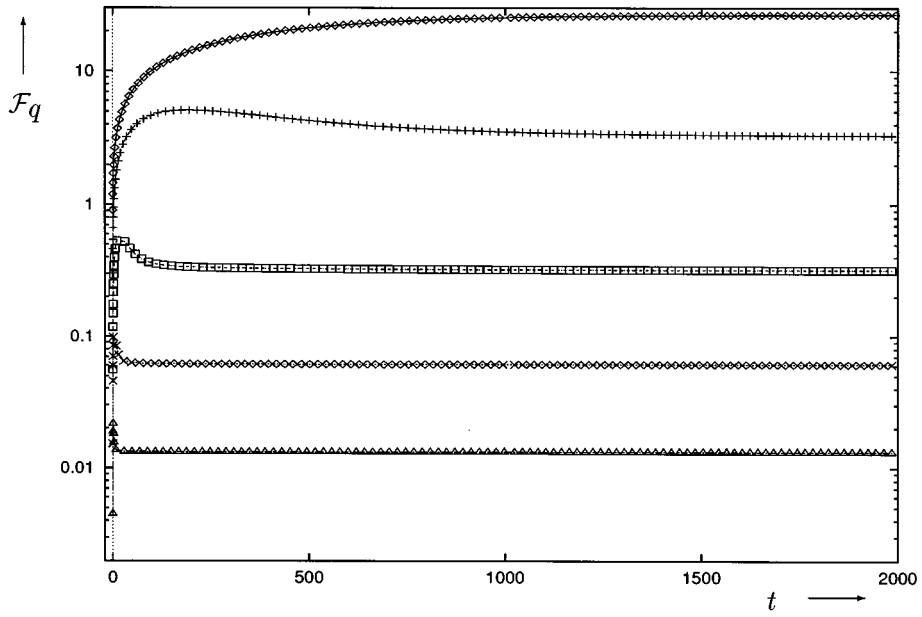

FIG. 18. Time evolution of the Fourier modes $\mathcal{F}_q$ for $q=1,2,5,10,20$ (from top to bottom) for flexible chain corresponding to the solid line in Fig. 15.

II′ are well visible from Fig. 17 (see, e.g., curve denoted by pluses).

We remark that, whereas the characteristic times for the collapse kinetics increase monotonically with the stiffness, for the unfolding they first increase and then start to decrease when λ becomes comparable to N (see Table VIII). The latter may be explained by the tendency of the stiffness effect to straighten the chain on larger scale.

IV. CONCLUSION

In this paper we have applied the Gaussian self-consistent method to the equilibrium and kinetic behavior of a stiff chain. The main results of the paper are as follows. At equilibrium we have obtained what we believe to be the generic phase diagram of stiff homopolymers (Fig. 1). The collapse transition for a sufficiently flexible polymer is second order. However, for higher stiffness it becomes first order and leads to formation of the toroidal globule. For stronger two-body attraction the torus can be transformed to the spherical globule via another first order transition. The toroidal phase therefore has a reentrant character in the solvent quality parameter. The transition lines intersect at a bicritical point, which determines the lower bound for the stiffness parameter permitting the torus. This is a novel phase transition phenomenon, emerging from the juxtaposition of a fractal and two different condensed phases. One can only suppose that new universal polymer exponents will be found in this regime. This problem deserves a deeper analysis by superior equilibrium theories than the mean-field theory we currently offer, and we are hopeful that other will take up that challenge.

TABLE VIII. Values of the characteristic times τ_m^μ, τ_t^μ, and τ_f^μ for the unfolding kinetics vs the degree of polymerization N for different values of the stiffness parameter λ. The initial and final values of the second virial coefficient are -40 and 15, respectively. Here the quantity γ denotes the exponent of the appropriate time for flexible chain in terms of the degree of polymerization, i.e., $\tau \sim N^\gamma$. Note that we have not attempted to estimate such exponents for stiff chain due to strong cross-over behavior.

N	30	50	70	100	150	γ
$\tau_m^\mu(\lambda=0)$	13.0	37.5	83.0	194.5	527.0	2.30 ± 0.08
$\tau_m^\mu(\lambda=2)$	15.7	87.7	258	710	2025	
$\tau_m^\mu(\lambda=6)$	9.18	71.0	264	960	3595	
$\tau_m^\mu(\lambda=15)$	4.80	42.5	180	795	3865	
$\tau_t^\mu(\lambda=0)$	72.91	263.7	610.6	1478	3981	2.49 ± 0.02
$\tau_t^\mu(\lambda=2)$	121.7	706.9	1934	4823	13080	
$\tau_t^\mu(\lambda=6)$	73.35	576.0	2084	7479	27800	
$\tau_t^\mu(\lambda=15)$	40.71	354.1	1440	6128	37000	
$\tau_f^\mu(\lambda=0)$	18.45	64.27	152.8	370.4	1002	2.49 ± 0.02
$\tau_f^\mu(\lambda=2)$	22.12	148.8	441.3	1105	3215	
$\tau_f^\mu(\lambda=6)$	10.56	86.51	349.5	1508	6452	
$\tau_f^\mu(\lambda=15)$	5.708	41.20	175.2	955.1	7965	

We have found that, for a given stiffness, there are lower and upper bounds on the chain length for the region of the torus stability. This conclusion is in accord with the mean field study of Ref. 28. We also agree with the latter work on the scaling of the torus radii on the stiffness: $R \sim r^{-1} \sim \lambda^{1/4}$, but with the earlier work[19] on the scaling in the chain length $R \sim R_g \sim N^{1/3}$.

It is worthwhile emphasizing that we have studied a microscopic model of a chain with a local mechanism of stiffness, while the previous mean field approaches are based on macroscopic approximate expressions for the free energy. These earlier works differ somewhat in their concrete predictions, but they are based on the general idea of competition between the bending and surface energies. Our equations at equilibrium yield the Gibbs–Bogoliubov variational estimate

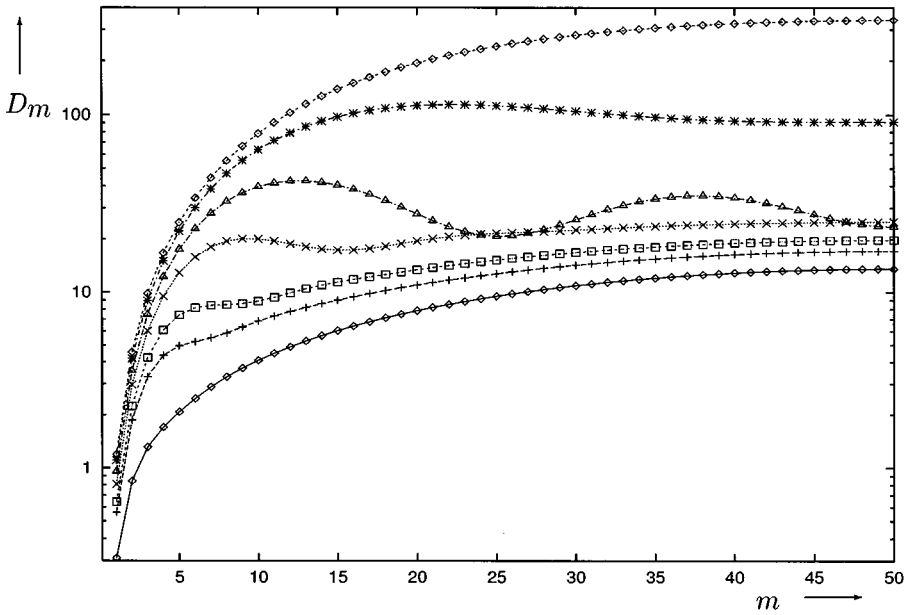

FIG. 19. Instantaneous profiles of the spatial correlations of monomer coordinates D_m vs the chain index m during kinetics corresponding to the line marked by pluses in Fig. 15 at different moments (from bottom to top): $t=0,0.2,1,10,500,2500,8000$.

that may be viewed as an optimised mean-field approximation, but with N variational parameters. One may expect this approach to be more accurate than several parametric mean-field theories. Moreover, we are able to describe the extended coil and the globular states within the same approximation. Significantly, the present method links the equilibrium theory with kinetics in a simple and intuitively transparent way. We view this a powerful argument in favor of using the statistical mechanical methods rather than only scaling theory in such a problem.

The correspondence between our statistical mechanics model and the phenomenological approaches previously developed is not completely obvious at the moment. One may not therefore expect a complete agreement between these two approaches as yet. Nevertheless, certain similarities in the predictions seem quite encouraging.

To finally resolve the equilibrium issues a better variational approach especially designed for studying the assymetrical globule may be constructed, even on the basis of non-Gaussian approximants. This would allow one to calculate the Gaussian topological invariant and analytically elucidate the relevant scalings using the dominant balance method and the Lorentzian *Anzatz* for the amplitudes of the internal modes. We hope to return to these interesting extensions of the method at a later stage.

In the present work our emphasis lays on the kinetics of conformational changes between different phases. One important conclusion is that the collapse kinetics can be trapped in a metastable state due to the first order character nature of some transitions. Hence the time evolution behaviour may become rather diverse depending on the system parameters. Nevertheless, the kinetics is quite well understood now in terms of the motion on the topographical map of the free energy and supported by direct calculation of relevant observables. This map has been examined by us in detail and classified according to the topological properties of the non-equilibrium states.

We have extracted the critical exponents ($\delta^{II''}_{-}=3/2$, $\delta^{III'}_{-}=\delta^{III''}_{-}=1/2$) describing the slowing down near the spinodal lines that separate regions of metastability. These exponents seem to be universal, albeit some of the scalings in terms of the chain size are probably not, as they might describe a crossover between flexible chain and rigid rod behaviors.

Finally, we believe that the present work might be of importance as a stage in the development of more realistic statistical model of DNA and other stiff biomolecules.[30] Evidently, in many cases DNA or other nucleic acids are more properly viewed as ribbons possessing additional energetic terms. However, in many other circumstances this is not an essential feature. In these cases one should understand the effect of rigidity on the problem, and our current work offers one an approach to this question that self-consistently addresses static and dynamic issues.

We have nevertheless identified a number of limitations in the study, beyond those inherent in the method itself. Thus electrostatic interactions are assumed to be well screened, and not dealt with here. It would be a relatively straightforward task to treat them along the lines discussed in Ref. 33. Second, we have implicitly assumed that the solvent quality can be described by static parameters, the virial coefficients, and in some recent experiments with slowly varying complexing agents[31] this is not the case. Clearly, some time dependence in the virial coefficients may have to be considered. Third, DNA, nor other stiff biopolymers are truly

homopolymers, though they are often approximated to be such. The virial coefficients and rigidity must in principle be considered to depend on the position along the chain. Since the chain is long, we may follow the same approach as that used in protein models and propose a statistical distribution of these parameters. If we do so, the information about the sequence distributions being brought forward by some researchers[32] can be of assistance. In any case, if we assume reasonable homogeneity in the virial coefficients, it seems that one might conjecture a variety of ''glassy'' states, driven by curvature energy heterogeneity.

There are numerous such avenues to be followed, and one hopes that this area will yield a rich source of interesting results for theoretical research. Also, a new stage of direct imaging of collapsing DNA molecules from fluorescence microscopy[31] will probably bring these issues more to the fore in nonequilibrium condensed phase science.

ACKNOWLEDGMENTS

The authors acknowledge interesting discussions with Professor A. Yu. Grosberg, Professor A. R. Khokhlov, Professor P. Pincus, Professor Y. Rabin, Professor K. Yoshikawa, Dr. A. V. Gorelov, and Dr. V. Vasilevskaya. One of us (K.A.D.) is grateful to the Canon Foundation for a visiting professorship which made it possible to discuss and observe fluorescence microscopy images of DNA collapse kinetics in the laboratory of Professor K. Yoshikawa.

[1] P. G. de Gennes, *Scaling Concepts in Polymer Physics* (Cornell University Press, Ithaca, 1988).
[2] J. des Cloizeaux and G. Jannink, *Polymers in Solution* (Clarendon, Oxford, 1990).
[3] M. Doi and S. F. Edwards, *The Theory of Polymer Dynamics* (Oxford Science, New York, 1989).
[4] A. Yu. Grosberg and A. R. Khokhlov, *Statistical Physics of Macromolecules* (AIP, New York, 1994).
[5] B. Ostrovsky and Y. Bar-Yam, Comput. Polym. Sci. **3**, 9 (1993); M. A. Smith, Y. Bar-Yam, Y. Rabin, B. Ostrovski, C. A. Bennett, N. Margolus, and T. Toffoli, Comput. Polymer Sci. **2**, 165 (1992).
[6] Yu. A. Kuznetsov, E. G. Timoshenko, and K. A. Dawson, J. Chem. Phys. **103**, 4807 (1995); **104**, 336 (1996).
[7] A. Byrne, P. Kiernan, D. Green, and K. A. Dawson, J. Chem. Phys. **102**, 573 (1995).
[8] T. A. Kavassalis and P. R. Sundrarajan, Macromolecules **26**, 4144 (1993); G. Tanaka and W. L. Mattice, *ibid*. **28**, 1049 (1995).
[9] P. G. de Gennes, J. Phys. Lett. **46**, L639 (1985).
[10] E. G. Timoshenko, Yu. A. Kuznetsov, and K. A. Dawson, J. Chem. Phys. **102**, 1816 (1995); K. A. Dawson, E. G. Timoshenko, and P. Kiernan, Nuovo Cimento D **16**, 675 (1994).
[11] Yu. A. Kuznetsov, E. G. Timoshenko, and K. A. Dawson, J. Chem. Phys. **104**, 3338 (1996).
[12] G. Allegra and F. Ganazzoli, J. Chem. Phys. **83**, 397 (1985).
[13] F. Ganazzoli, R. La Ferla, and G. Allegra, Macromolecules **28**, 5285 (1995).
[14] This equation fundamentally represents a phantom ''network,'' which can pass through itself. We note that this is not the same as a phantom chain, and the fact that there are effective springs connected between all pairs has the effect of restraining crossing. The effect of nonphantomness has been studied in Monte Carlo simulation for a homopolymer in Ref. 33. It is quite important in the dense globular[34] state. For an open polymer topological restrictions may be removed via self-reptations of the chain, and it has been argued that this leads to an even longer final kinetic stage with the time scale $\tau_{\text{reptations}} \sim N^3$.
[15] Without hydrodynamics the friction becomes a constant $\zeta_q = \zeta_b N$, where ζ_b is the bare mobility of monomers. Henceforth we shall disregard the hydrodynamic interaction, which could be easily incorporated into our scheme and discussed in detail in Ref. 11.
[16] E. G. Timoshenko, Yu. A. Kuznetsov, and K. A. Dawson, Phys. Rev. E **53**, 3886 (1996); *ibid*. (in press).
[17] V. A. Bloomfield, Biopolymers **31**, 1471 (1991); J. Ubbink and T. Odijk, Biophys. J. **68**, 54 (1995); Europhys. Lett. **33**, 353 (1996); N. V. Hud, K. H. Downing, and R. Balhorn, Proc. Natl. Acad. Sci. USA **92**, 3581 (1995).
[18] L. S. Lerman, Proc. Natl. Acad. Sci. USA **68**, 1886 (1971); U. K. Laemmli, *ibid*. **72**, 4288 (1975); Yu. M. Evdokimov *et al.*, Nucl. Acids Res. **3**, 2353 (1976); G. E. Plum, P. G. Arscott, and V. A. Bloomfield, Biopolymers **30**, 631 (1990); V. V. Vasilevskaya, A. R. Khokhlov, Y. Matsuzawa, and K. Yoshikawa, J. Chem. Phys. **102**, 6595 (1995).
[19] A. Yu. Grosberg, Biophysics **24**, 30 (1979); A. Yu. Grosberg and A. R. Khokhlov, Adv. Polym. Sci. **41**, 53 (1981).
[20] O. Kratky and G. Porod, Rec. Trav. Chim. **68**, 1106 (1949); H. Yamakawa, Annu. Rev. Phys. Chem. **35**, 23 (1984).
[21] R. A. Harris and J. E. Hearst, J. Chem. Phys. **44**, 2595 (1966).
[22] B. H. Zimm, J. Chem. Phys. **24**, 269 (1956); M. V. Volkenstein, *Configurational Statistics of Polymeric Chains* (Interscience, New York, 1963); P. J. Flory, *Statistical Mechanics of Chain Molecules* (Interscience, New York, 1969); M. Bixon and R. Zwanzig, J. Chem. Phys. **68**, 1896 (1978); A. Perico, S. Bisio and C. Cuniberti, Macromolecules **17**, 2686 (1984).
[23] Formulas for an open polymer may be found in Ref. 11.
[24] Note that the Gaussian trial Hamiltonian has the flaw that the extended coil has an incorrect (Reiss) swelling exponent $\nu = 2/3$, unless one makes a specific cut-off (Ref. 35).
[25] Whilse the interpretation of $D_{\max}$ as the mean squared *extrinsic* diameter of the torus is fairly well justified, for $D_{\min}$ one can, strictly speaking, say that it is connected to the mean squared *intrinsic* diameter only up to some multiplicative factor, depending on many details of the local interaction.
[26] Since for a finite size system this continuous transition occurs in a region of width $\sim 1/N$, the transition line is not so well defined. Practically, curve *I* has been obtained as the point of the most rapid decrease of the radius of gyration.
[27] Note that the squared radius of gyration for the torus is somewhat smaller than for the spherical globule in close vicinity of the transition region. This is related to that the spherical globular state is more optimized with respect to the volume to surface ratio determining the balance of the attractive two-body and repulsive three-body interactions for a given values of the thermodynamical parameters u_2 and u_3.
[28] V. V. Vasilevskaya, A. R. Khokhlov, S. Kidoaki, and K. Yoshikawa (unpublished).
[29] E. G. Timoshenko and K. A. Dawson, Phys. Rev. E **51** (1), 492 (1995).
[30] H. Isambert, A. C. Maggs, Macromolecules **29**, 1036 (1996).
[31] S. Kidoaki and K. Yoshikawa *et al.* (unpublished).
[32] H. E. Stanley *et al.*, Nuovo Cimento D **16**, 1339 (1994).
[33] A. Yu. Grosberg, Yu. A. Kuznetsov, E. G. Timoshenko, and K. A. Dawson (unpublished).
[34] A. Yu. Grosberg and D. V. Kuznetsov, Macromolecules **26**, 4249 (1993).
[35] D. Bratko and K. A. Dawson, J. Chem. Phys. **99**, 5352 (1993).